Distribution Category:
Energy Conservation—
Industry (UC-95f)

ANL-83-8

ANL--83-8

DE83 007812

ARGONNE NATIONAL LABORATORY
9700 South Cass Avenue
Argonne, Illinois 60439

FLUIDELASTIC INSTABILITY IN SHELL AND TUBE HEAT EXCHANGERS - A FRAMEWORK FOR A PREDICTION METHOD

by

M. W. Wambsganss, C. I. Yang, and H. Halle

Components Technology Division

DISCLAIMER

December 1982

TABLE OF CONTENTS

		Page
ABSTRACT		7
I.	INTRODUCTION	9
II.	EXCITATION MECHANISMS	10
III.	FRAMEWORK FOR PREDICTION METHOD	15
	A. Flow Distribution	15
	B. Local Crossflow Velocity	16
	C. Tube Vibration Frequencies and Modes	19
	D. Reduced Effective Crossflow Velocity	21
IV.	APPLICATION	22
	A. Description of Heat Exchanger	22
	B. Partitioning of Computational Mesh	22
	C. COMMIX-IHX/SG Input/Output	26
	D. Vibration Analysis	28
V.	EVALUATION OF RESULTS	38
	A. Qualitative Comparison with Experimental Results	38
	B. Quantitative Comparison with Laboratory Results and Design Guides	45
VI.	CONCLUDING REMARKS AND RECOMMENDATIONS	51
ACKNOWLEDGMENTS		52
REFERENCES		53

LIST OF FIGURES

No.	Title	Page
1	Stability diagram for triangular arrays.....	13
2	Typical computational cell.....	17
3	Computational cell map in r-θ plane.....	18
4	Computation of local tube crossflow velocity from cell data...	20
5	Argonne test heat exchanger in seven-baffle/eight-crosspass configuration.....	23
6	Layout of heat exchanger tube bundle.....	25
7	Computational cell map in r-z plane.....	27
8	Flow pattern in r-z plane at J-section 3-9 (a cross-section through the centerline of the inlet/outlet nozzle).....	30
9	Flow pattern in r-θ plane at axial location K = 3.....	31
10	Flow pattern in r-θ plane at axial location K = 5.....	32
11	Computer output for resultant crossflow velocity distributions for flow past tube V-24.....	33
12	Computer output for resultant crossflow velocity distributions for flow past tube Z-24.....	34
13	Resultant crossflow velocity distribution for flow past tube V-24.....	35
14	Theoretical tube vibration mode shapes and frequencies, with water on shellside; n = 1-6.....	36
15	Reduced effective flow velocities for tubes in window regions; 7-baffle configuration, Q = 3,300 gpm.....	39
16	Reduced effective flow velocities for tubes in window regions; 5-baffle configuration, Q = 2,000 gpm.....	40
17	Experimental data from tube vibration test [5]: ⊗ - tube with large amplitude vibration; 7-baffle configuration.....	41
18	Tubes with high values of reduced effective flow velocities; 7-baffle configuration, Q = 3,300 gpm.....	42
19	Tubes with high values of reduced effective flow velocities; 5-baffle configuration, Q = 2,000 gpm.....	44

20 Predicted values of reduced effective flow velocity extrapolated to average critical flow rate for the particular window region; 7-baffle configuration..... 49

21 Predicted values of reduced effective flow velocity extrapolated to average critical flow rate for the particular window region; 5-baffle configuration..... 50

LIST OF TABLES

No.	Title	Page
1	Lower bound on critical flow velocity.....	14
2	Description of heat exchanger.....	24
3	Sample output: u and v velocities for cells (I, J, 6).....	29
4	Sample results: Reduced effective crossflow velocities ($\bar{U}_n$) - 7-baffle configuration, Q = 3,300 gpm.....	37
5	Experimental values of critial flow rate and extrapolation factor K' based on the average critical flow rate.....	47

NOMENCLATURE

d	Tube diameter
f	Natural frequency of tube
f_n	Natural frequency of nth vibration mode
I,J,K	Indices identifying computational cells
ℓ	Overall tube length
m	Mass of tube per unit length
p	Pressure at computational cell center
P	Tube layout pitch
Q	Volumetric flowrate through heat exchanger
r,θ,z	Cylindrical coordinates
u,v,w	r, θ, and z components of velocity, respectively
u_T,v_T	Velocity components interpolated to tube locations
U	Crossflow velocity
$\bar{U}$	Reduced crossflow velocity
U_{en}	Effective crossflow velocity
$\bar{U}_n$	Reduced effective crossflow velocity
$\bar{U}_r$	Dimensionless critical velocity
V	Resultant crossflow velocity
z	Position along length of tube
α	Instability constant for fluidelastic-stiffness-controlled instability
β	Instability constant for fluid-damping-controlled instability
δ_m	Mass-damping parameter
ζ	Equivalent viscous damping factor
ρ	Mass density of shellside fluid
ϕ_n	nth vibration mode

FLUIDELASTIC INSTABILITY IN SHELL AND TUBE HEAT EXCHANGERS - A FRAMEWORK FOR A PREDICTION METHOD

by

M. W. Wambsganss, C. I. Yang, and H. Halle

ABSTRACT

Criteria for predicting the threshold of fluidelastic instability in heat exchanger tube bundles have been developed from ideal, laboratory tests and in application require, among other things, an effective crossflow velocity. This characteristic velocity is obtained from a vibration mode weighted average of the spanwise crossflow velocity distribution and will, in general, be different for each tube and each vibration mode. Because of the complexities of the flow pattern within a segmentally baffled exchanger, its dependence on design features, and the requirement for detailed velocity data, the need to rely on a numerical simulation of the three-dimensional flow velocity field is identified. A framework for a method to predict fluidelastic instability in heat exchanger tube bundles is presented. The method relies on a three-dimensional, cylindrical coordinate, thermal-hydraulic analysis code to obtain a representation of the three-dimensional flow distribution within the heat exchanger. With this information, local crossflow velocities corresponding to each tube in the exchanger are obtained by interpolation and resultant crossflow velocity distributions are computed. With a knowledge of the vibration mode shapes and frequencies, reduced effective crossflow velocities are then computed for each tube. A comparison with experimental results shows excellent agreement: the tubes with high values of predicted reduced effective crossflow velocity are the same tubes that first experience fluidelastic instability in the flow tests and vibrate most violently; also, the simulation correctly predicts that the tubes directly exposed to the flow from the inlet nozzle have a low potential for fluidelastic instability. Very good agreement is also shown in the comparison of the predicted reduced effective crossflow velocities with the critical value obtained from a design guide. In summary, the feasibility of developing a heat exchanger tube vibration prediction method, based on a computer simulation of flow distribution, is demonstrated. Such a method would have immediate application in design optimization. However, further development and evaluation are required.

I. INTRODUCTION

Flow-induced vibration of heat exchanger tubes has resulted in tube failures caused by mechanical wear, fretting corrosion, and fatigue cracking. The detrimental effects of tube vibration failures, including costly plant shutdowns, have motivated numerous investigations. These investigations include a DOE-sponsored Heat Exchanger Tube Vibration Program [1], established at Argonne National Laboratory, with the objectives (1) to obtain tube vibration data under controlled conditions from tests of specially built and instrumented, industrial-type, shell-and-tube heat exchangers, (2) to obtain tube vibration data from field experiences collected and subsequently entered into a data bank, and (3) to use the above data to further the understanding of tube-excitation mechanisms and to evaluate and improve current predictive methods and design guidelines.

Tubes in a segmentally-baffled, shell-and-tube heat exchanger are exposed to a complex shellside flow pattern that reverses itself as the fluid flows from inlet to outlet. The flow field includes significant axial components of velocity. However, it is the crossflow components that possess the strongest potential for exciting vibration through such mechanisms as vortex shedding, turbulent buffeting, and fluidelastic instability.

There are various methods and criteria available for designing heat exchangers to avoid detrimental tube vibration. Many of the early methods were simply design rules-of-thumb that evolved with experience. At the time, tube vibrations were poorly understood. Today, the excitation mechanisms are better understood and improved design methods have been developed [e.g., 2-4] based, in most cases, on laboratory tests involving uniform flow. Virtually all of these design methods require, as an input parameter, a characteristic crossflow velocity. However, in application, because of the complex flow distribution, the designer is faced with the problem of how to define and calculate this characteristic velocity. Inlet/outlet nozzle sizes, impingement plates, baffle size and spacing, and leakage paths, both between shell and tube bundle and between tubes and baffle plate holes, all will affect the flow velocity distribution.

Results from the tube vibration test program at Argonne [5-7] have indicated that specific groups of tubes in the "window" regions,* notably those in the first row after the baffle cut and those where the baffle and shell meet, tend to experience fluidelastic instability first, as flow rate

*The window regions are defined as those regions of a segmentally-baffled tube bundle in which the tubes are not supported by every baffle.

is increased, and to vibrate most violently. This would indicate that there are relatively high local crossflow velocities in these regions. The identification and characterization of these high velocity regions in a given heat exchanger design are important from the standpoint of evaluating the potential for tube vibration and for providing field fixes (such as removing selected groups of tubes to create passlanes).

There are very limited experimental data available in the open literature on flow distribution in actual heat exchangers. This is due, in large part, to the difficulty, not to mention the expense, in making meaningful three-dimensional flow velocity measurements within a tightly packed tube bundle without significantly disturbing the local flow field with the probe and, thereby, affecting the velocity measurement. Further, the flow field can be expected to be dependent on minor design changes involving the baffles, leakage paths, and tube layout. It would be prohibitively expensive to perform a flow distribution test to evaluate each design modification.

To satisfy this need for detailed knowledge of the crossflow velocities and to circumvent the need for expensive flow tests, an experimentally-validated computer code, capable of predicting three-dimensional flow velocity fields, is required.

In the study reported herein, a framework of a method to predict fluidelastic instability in actual heat exchanger tube bundles is presented. The method is based on results obtained from a three dimensional thermal-hydraulic code. From a gross simulation of flow distribution, linear interpolation is used to calculate a crossflow velocity distribution for each tube in the heat exchanger. With this information, and knowledge of the tube mode shapes and frequencies, a reduced effective flow velocity is predicted for each tube in the exchanger. A preliminary comparison with experimental results is made to evaluate the ability of the procedure to predict which groups of tubes are expected to experience the highest levels of fluidelastic instability.

II. EXCITATION MECHANISMS

The dynamic behavior of a heat exchanger tube bundle, as the shellside flow rate is increased, can be summarized as follows: At low flow rates small-amplitude tube motions, typically random in nature, occur; these increase to cause rattling within the baffle (support) plate hole as the flow rate is increased; large amplitude motion and possible tube-to-tube impacting results when the flow rate exceeds a threshold value. The three mechanisms generally regarded as responsible for the vibration of heat

exchanger tubes are (1) turbulent buffeting, (2) vortex shedding, and (3) fluidelastic instability.

Turbulent buffeting is present at all flow rates and includes random pressure fluctuations associated with the turbulent boundary layer, as well as turbulent wake flows from upstream tubes. In general, it is random in nature and can be considered responsible for the low-level tube vibration and rattling experienced at subcritical (below the threshold flow rate for large amplitude vibration) flow rates. Vortex shedding, while an important mechanism for single cylinders exposed to crossflow, is generally not important for a tube bundle unless the tube spacing is large (pitch-to-diameter ratio, P/d > 2.0 [8]); for most industrial heat exchangers the spacing is relatively small with typical values of P/d ranging from 1.25 to 1.40. The mechanism of most concern is fluidelastic instability, as it leads to large amplitude motion that persists once the threshold flow rate is exceeded.

Fluidelastic instability, of the type responsible for tube bundle vibration, was first reported by Connors [9] and subsequently has been the subject of a considerable number of investigations, both experimental [e.g., 10-16] and theoretical [e.g., 17-21]. Recently Chen [18,19] used a mathematical model to show that there are two distinct instability mechanisms: a velocity mechanism, which results in a fluid-damping-controlled instability; and a displacement mechanism, which results in a fluidelastic-stiffness-controlled instability.

In general, both fluidelastic and fluid damping forces contribute to the dynamic instability. While a closed form solution cannot be obtained for the general case, the instability criterion can be written in functional form as

$$\left(\frac{U}{fd}\right) = F\left(\frac{m}{\rho d^2}\ ,\ \zeta,\ \frac{P}{d}\ ,\ \text{turbulence characteristics}\right) . \qquad (1)$$

In gas flows the instability is often dominated by the displacement mechanism and is fluidelastic-stiffness-controlled. The instability occurs at high reduced flow velocities. In this range, the fluidelastic coefficients are independent of the reduced flow velocity and fluid damping coefficients are proportional to the reduced flow velocity. The stability criterion can be written in closed form as

$$\left(\frac{U}{fd}\right) = \alpha\left(\frac{2\pi\zeta m}{\rho d^2}\right)^{0.5} , \qquad (2)$$

where α is a constant for a given tube array. Equation (2) is valid for

both fluid-damping-controlled and fluidelastic-stiffness-controlled instability at high reduced flow velocity region.

In liquid flows the instability mechanism is often fluid-damping-controlled and attributed to the velocity mechanism. The instability occurs at low reduced flow velocities; in this range, the fluid force coefficients are functions of the reduced flow velocity. The stability criterion can be written as

$$\left(\frac{U}{fd}\right) = \beta\left(\frac{2\pi\zeta m}{\rho d^2}\right) , \tag{3}$$

where β is a function of the reduced flow velocity $\bar{U}$ (= U/fd).

In application of Eqs. (2) and (3), Chen points out that theoretically either the in-vacuo values or in-fluid values of m, f, and ζ can be used in the stability equations.

While significant progress is being made in developing an understanding of fluidelastic instability phenomena in tube bundles, the state-of-the-art has not yet progressed to the point which would allow calculation of the fluid dynamic force coefficients required for evaluation of the flow-velocity and geometry dependent coefficients, α and β, in Eqs. (2) and (3). Consequently, in design, it is still necessary to rely on experimental data obtained from laboratory tests. In a recently published design guide [22], Chen has assembled available experimental data and has plotted a dimensionless critical flow velocity as a function of the mass-damping parameter $\delta_m (= 2\pi\zeta m/\rho d^2)$ for each of several standard tube layouts. Chen then established lower bounds for the data and, thereby, obtained a set of stability diagrams; see, for example, Fig. 1. For the 30° triangular layout presented in Fig. 1, the dimensionless critical flow velocity is defined as

$$\bar{U}_r = \frac{(U/fd)}{2.105\ (P/d - 0.9)} . \tag{4}$$

Table 1, adapted from Ref. 22, gives these lower bounds in equation form for five different tube array geometries. It should be noted that in application of the stability criteria, the frequency associated with the tube bundle submerged in the shellside fluid should be used in computing the reduced flow velocity.

Application of the stability criteria given in Eqs. (2) and (3), or that given in Table 1, to the design evaluation of an actual heat exchanger is complicated by the complexities of the flow distribution within the heat exchanger, not to mention inherent uncertainties and nonlinearities related to the degree of tube support provided by the baffles that will affect tube vibrational characteristics. In particular, the empirical correlations are

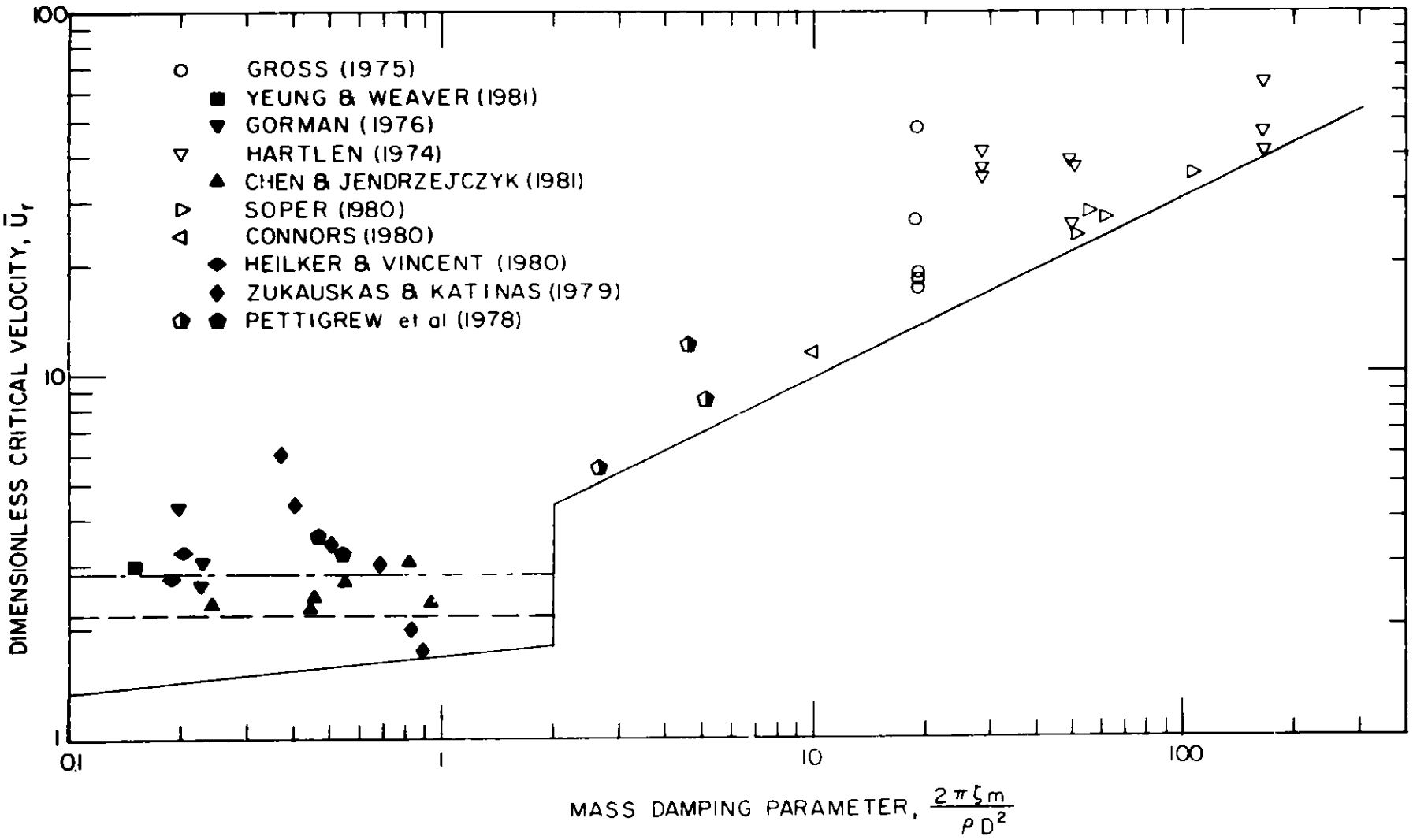

Fig. 1. Stability diagram for triangular arrays [22]; — — — revised lower bound; — - — average through experimental data

Table 1. Lower bound on critical flow velocity (from Ref. 22)

Array	Parameter Range for δ_m	$\frac{U_m}{fd}$
Tube Row	$0.05 < \delta_m < 0.3$	$1.35(P/d - 0.375)\delta_m^{0.06}$
	$0.3 < \delta_m < 4.0$	$2.30(P/d - 0.375)\delta_m^{0.5}$
	$4.0 < \delta_m < 300$	$6.00(P/d - 0.375)\delta_m^{0.5}$
Square (90°)	$0.03 < \delta_m < 0.7$	$2.10\ \delta_m^{0.15}$
	$0.7 < \delta_m < 300$	$2.35\ \delta_m^{0.48}$
Rotated Square (45°)	$0.1 < \delta_m < 300$	$3.54(P/d - 0.5)\delta_m^{0.5}$
Triangular (30°)	$0.1 < \delta_m < 2$	$3.58(P/d - 0.9)\delta_m^{0.1}$
	$2 < \delta_m < 300$	$6.53(P/d - 0.9)\delta_m^{0.5}$
Rotated Triangular (60°)	$0.01 < \delta_m < 1$	$2.8\ \delta_m^{0.17}$
	$1 < \delta_m < 300$	$2.8\ \delta_m^{0.5}$

developed for the case in which the entire tube length is exposed to a uniform crossflow. In an actual heat exchanger the flow is highly nonuniform, as it is directed through the exchanger by the baffles, and will vary with location in the tube bundle. Consequently, it is necessary to define a characteristic, or effective, crossflow velocity which serves to reduce the general case of nonuniform flow to the ideal case of uniform flow.

An effective, or equivalent, uniform, flow velocity used by many investigators is defined as

$$U_{en} = \frac{\left[\int_0^{\ell} V^2(z)\phi_n^2(z)dz\right]^{1/2}}{\int_0^{\ell} \phi_n^2(z)dz} \tag{5}$$

where $V(z)$ is the distributed flow velocity and $\phi_n(z)$ is the nth vibration mode. Chen has shown that Eq. (5) is applicable if (1) the fluidelastic coefficients are constant (α = constant in Eq. (2)), and (2) the fluid-damping coefficients are proportional to the reduced flow velocity ($\beta \propto \bar{U}$ in Eq. (3)). These two conditions are satisfied at high reduced flow velocities (high values of mass-damping parameter) and, therefore, Eq. (5) is applicable for the case of gas flows. While not strictly applicable for liquid flows, which are associated with low reduced flow velocities, for the purpose of this investigation it will be assumed that Eq. (5) is, nevertheless, still a reasonable method for computing an effective flow velocity for a segmentally-baffled, shell-and-tube heat exchanger. Tube instability then results when the reduced effective flow velocity $\bar{U}_n (= U_{en}/f_n d)$ exceeds the critical value determined from stability diagrams, such as Fig. 1, or empirical stability relationships (see, for example, Table 1).

Computation of a reduced effective flow velocity requires knowledge of the local crossflow velocity distribution $V(z)$, as well as the tube vibrational natural frequencies and associated modes.

III. FRAMEWORK FOR PREDICTION METHOD

A. Flow Distribution

Flow distribution in a heat exchanger can be obtained by measurement. However, because of the close spacing of the tubes within the bundle, it is typically a difficult measurement to make; for example, the presence of the measuring probe can be expected to locally disturb the flow field and, thereby, give an erroneous reading. Also, a very large number of measurements is required to adequately represent the flow field. Such a

measurement program would be very expensive and time-consuming. Furthermore, the program would have to be repeated for every new design and/or design modification.

An alternative, and more attractive, approach is to employ an analytical prediction method. This approach has become feasible with the advent of large digital computers and advances in the development of computational fluid mechanics. Typically the approach is to divide the heat exchanger into a number of computational cells and to numerically solve the complex conservation equations of mass, momentum, and energy. One such three-dimensional, thermal-hydraulic computer code, developed for the analysis of shell-and-tube heat exchangers for liquid metal service, is COMMIX-IHX/SG [23].

COMMIX-IHX/SG uses the concepts of volume porosity (fraction of volume occupied by fluid in the control volume), surface permeability factor (fraction of open projected flow area in the direction of flow component in the control volume), and distributed resistance (pressure loss term in the direction of flow component through submerged obstacles such as flow baffles and tube support plates) to account for the blockage effects due to the presence of the tubes, flow baffles/shrouds, support plates, and the like. In application, the heat exchanger is partitioned into a number of computational cells in a cylindrical arrangement; a typical cell is shown schematically in Fig. 2. For each cell the code predicts the radial (u), azimuthal (v), and axial (w) velocities, and the pressure (p). The computed values of these quantities are for specific locations on the surface of, or within, the cell as illustrated in Fig. 2; indices I, J, K define the cell and refer to the r, θ, z dimensions, respectively. In this manner, the code generates a simulation of the flow distribution. Theoretically, the finer the mesh, the more detailed (accurate) the flow simulation will be. However, the computational time, and, hence, cost, will increase substantially with an increase in the number of cells employed in the simulation and a trade-off between accuracy and cost must be established.

B. Local Crossflow Velocity

In predicting the fluidelastic instability threshold of a tube bundle, it is the crossflow components of flow velocity, viz., radial velocity (u) and azimuthal velocity (v), that are of most importance. COMMIX-IHX/SG predicts flow velocities at only a relatively small number of points in a cross-sectional plane: the cell boundaries.

Each cell will contain a number of tubes, with the number increasing with the distance of the cell from the center of the exchanger; see, for example, the computational cell map in the r-θ plane given in Fig. 3.

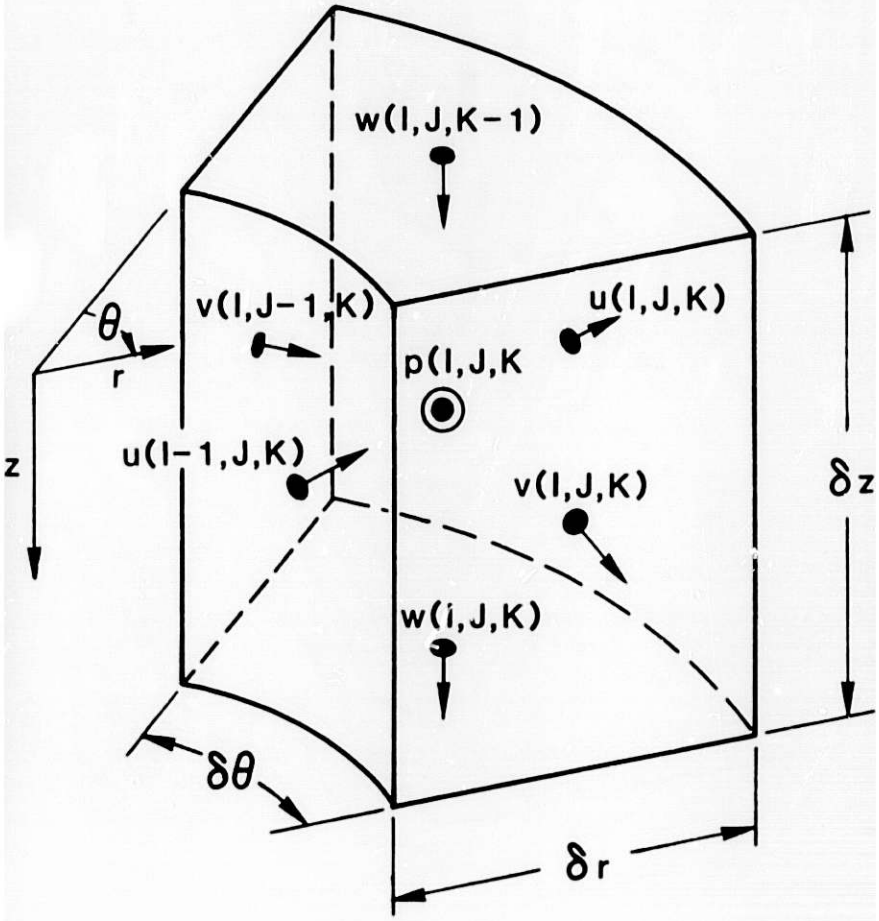

Fig. 2. Typical computational cell

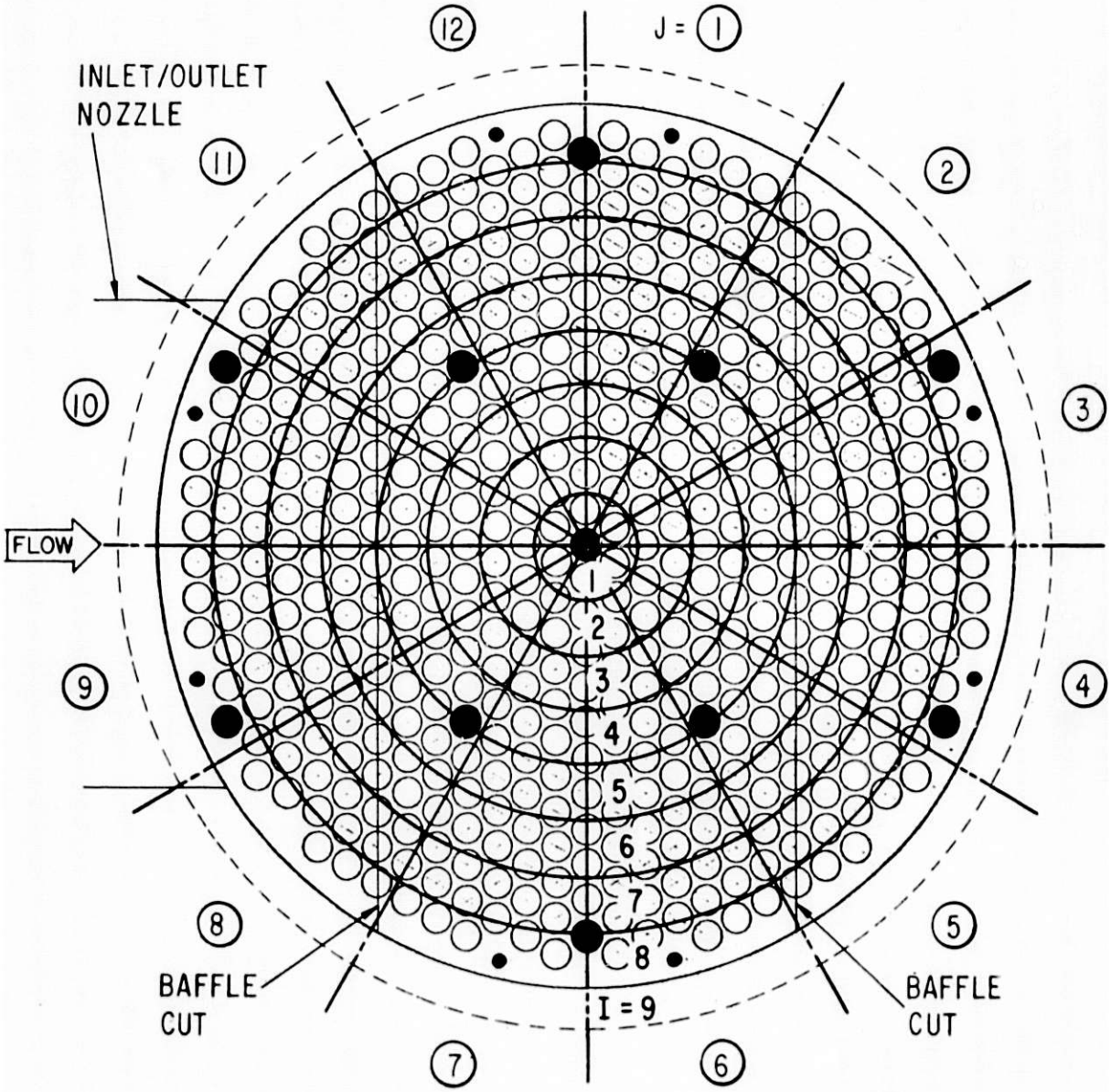

Fig. 3. Computational cell map in r-θ plane

Knowing the flow velocities at the cell boundaries, the local velocities corresponding to a particular tube location can be most easily approximated using linear interpolation. This is the method employed herein.

With reference to Fig. 4a, the local u-component of crossflow velocity u_T for a tube positioned as shown relative to the centers of adjacent computational cells can be estimated as

$$u_T = (1 - s)[t \cdot u(I,J+1,K) + (1 - t)u(I,J,K)]$$

$$+ s[t \cdot u(I+1,J+1,K) + (1 - t)u(I+1,J,K)] \ . \qquad (6)$$

Similarly, with reference to Fig. 4b, the local v-component of crossflow velocity v_T for a given tube location can be estimated as

$$v_T = \bar{s}[\bar{t} \cdot v(I+1,J+1,K) + (1 - \bar{t})v(I+1,J,K)]$$

$$+ (1 - \bar{s})[\bar{t} \cdot v(I,J+1,K) + (1 - \bar{t})v(I,J,K)] \ . \qquad (7)$$

Given these approximations, it is possible to calculate $u_T(z)$ and $v_T(z)$ where z denotes the cell center in the z-direction (Index K). The local crossflow velocities can be computed in this manner for every tube within the heat exchanger.

The flow distribution V(z) to be used in Eq. (5) to compute the effective flow velocity is taken to be the vector sum of the local velocities $u_T(z)$ and $v_T(z)$, obtained as

$$V(z) = [u_T^2(z) + v_T^2(z)]^{1/2} \ ; \qquad (8)$$

see Fig. 4c. It is recognized that the vector V(z) will not lie in a single plane and, thereby, represent an ideal, unidirectional, crossflow velocity distribution. Nevertheless, it is felt that the magnitude of the crossflow vector, as given by Eq. (8), provides a good indicator of the amount of energy in the flow, available for inducing and sustaining the large amplitude tube vibration associated with fluidelastic instability. An indication of angular variation of the direction of the resultant velocity with respect to distance along the tube length can be obtained from the ratio u/v.

C. Tube Vibration Frequencies and Modes

With a knowledge of the velocity distribution V(z) for each tube within the heat exchanger, the remaining information required to calculate an equivalent uniform flow velocity, according to Eq. (5), is knowledge of the

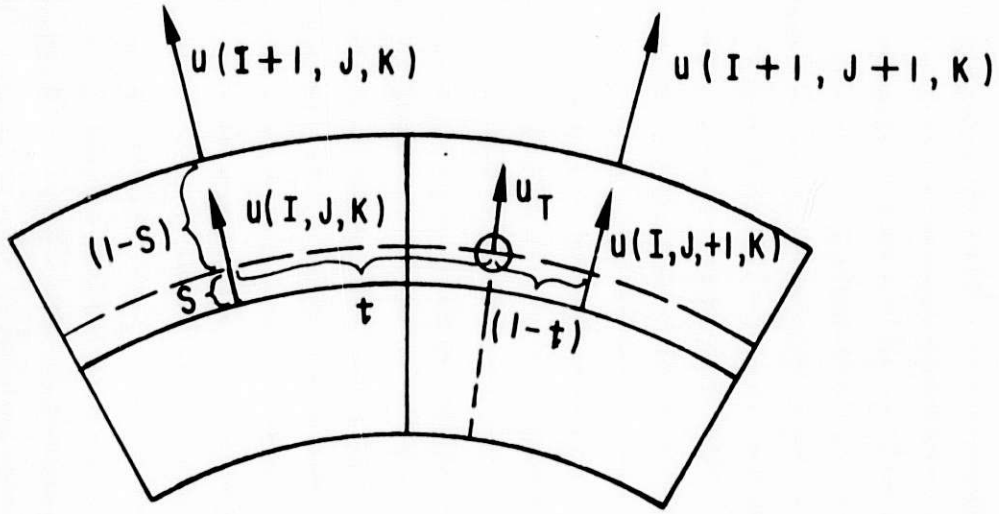

(a) Determination of $u_T(z)$

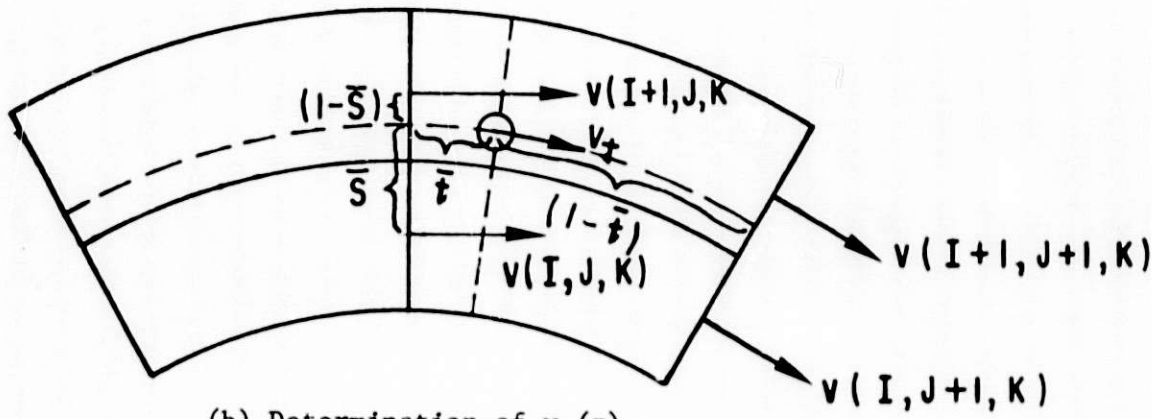

(b) Determination of $v_T(z)$

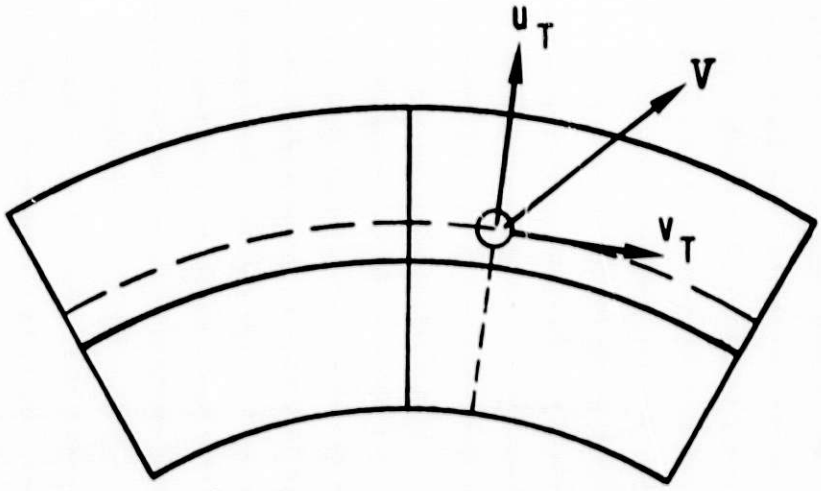

(c) Resultant crossflow velocity

Fig. 4. Computation of local tube crossflow velocity from cell data

tube vibrational modes $\phi_n(z)$. Computation of tube vibration natural frequencies and modes requires assumptions for the boundary conditions. In this regard, the results of several investigations have led to the conclusion that, with the exception of the combination of short spans and relatively large tube to baffle hole clearances (say, >20 mils), it is reasonable to assume that the baffle plates act as "knife-edge" supports [24,25]. It might be noted that the combination of short spans and large clearances makes it possible for a tube to "float" in the baffle hole such that the baffle is inactive as a support. In such cases the potential for fluidelastic vibration can be checked by assuming select baffles to be inactive or, in effect, absent. At the tubesheet a fixed boundary condition is typically assumed.

There are a number of computer codes available for predicting the vibrational characteristics of a beam with intermediate supports. The code selected for use in this study is BEAMINT [26]. The method used in the code involves a modification of the Rayleigh-Ritz method, used in conjunction with Lagrangian multipliers, Fourier cosine series, and Stokes' transformation. It provides an exact solution for the natural frequencies and modes.

D. Reduced Effective Crossflow Velocity

A numerical integration scheme is employed to compute the integrals in Eq. (5), thereby, allowing calculation of the effective crossflow velocity. A reduced effective crossflow velocity is calculated by dividing the effective crossflow velocity by the product of the appropriate natural frequency and tube diameter. For each tube in the heat exchanger, there will be a number of reduced effective crossflow velocities corresponding to each axial tube vibration mode. Maps of the tube bundle depicting the reduced effective crossflow velocity can be developed. It should be noted that the largest values of reduced effective crossflow velocity will not necessarily correspond with the lowest tube vibrational mode.

Qualitatively, the tubes having the highest value of reduced effective crossflow velocity have the greatest potential for going unstable and would be expected to experience instability first, as the shellside flow rate is increased. Quantitatively, the computed value of reduced effective crossflow velocity can be compared with the lower bound critical value obtained from application of the appropriate stability design guides as given in Fig. 1, for a 30° triangular layout, and Table 1. Tube instability can be expected when the computed value of reduced effective crossflow velocity exceeds the critical value.

IV. APPLICATION

The Argonne test heat exchanger is a segmentally-baffled, industrial-size unit designed for the purpose of obtaining tube vibration data under controlled conditions [5-7]. Tube vibrational behavior, in particular, the onset of fluidelastic instability, has been studied in detail for several tube layouts and various tube bundle configurations. Results for an equilateral (30°) triangular layout and tube bundle configurations consisting of seven-baffle/eight-crosspass and five-baffle/six-crosspass arrangements have been reported in Refs. 5 and 7, respectively. To evaluate the feasibility of the prediction method outlined in Section III, the method was applied to these two configurations of the test exchanger. Discussion in this section focuses on the seven-baffle/eight-crosspass configuration as an example.

A. Description of Heat Exchanger

The Argonne test heat exchanger is described in detail in Ref. 5. The exchanger is designed such that it can be readily disassembled and reassembled to obtain the configurations necessary to provide various test parameters affecting tube natural frequency, flow conditions, and tube pattern. The seven-baffle/eight-crosspass configuration is illustrated schematically in Fig. 5; pertinent dimensions are given in Table 2. The shellside fluid is water. The tubes are open to the atmosphere with no tubeside flow. A 30°-triangular tube layout is illustrated in Fig. 6.

For the various configurations tested, the baffle plates are nominally equally-spaced along the length of the unit. It should be noted that for the shell-nozzle configuration in which both inlet and outlet nozzles are on the same side as in Fig. 5, the baffle arrangement gives rise to three different tube support configurations. A "window" region is defined as a region in the tube bundle in which the tubes are not supported by every baffle; see Fig. 5. In general, if there are n baffles, in a configuration with an odd number of baffles, the tubes will be supported by $(\frac{n-1}{2})$, $(\frac{n+1}{2})$, or n baffles, depending on whether a tube is located in the far-window region (window region opposite the inlet nozzle), near-window region (window region adjacent to inlet nozzle), or non-window region, respectively.

B. Partitioning of Computational Mesh

Numerical simulation requires that the heat exchanger be partitioned into a number of computational cells (see Fig 2, for a typical cell schematic) in a cylindrical coordinate arrangement. To enforce certain boundary conditions, COMMIX-IHX/SG further requires that an extra layer of

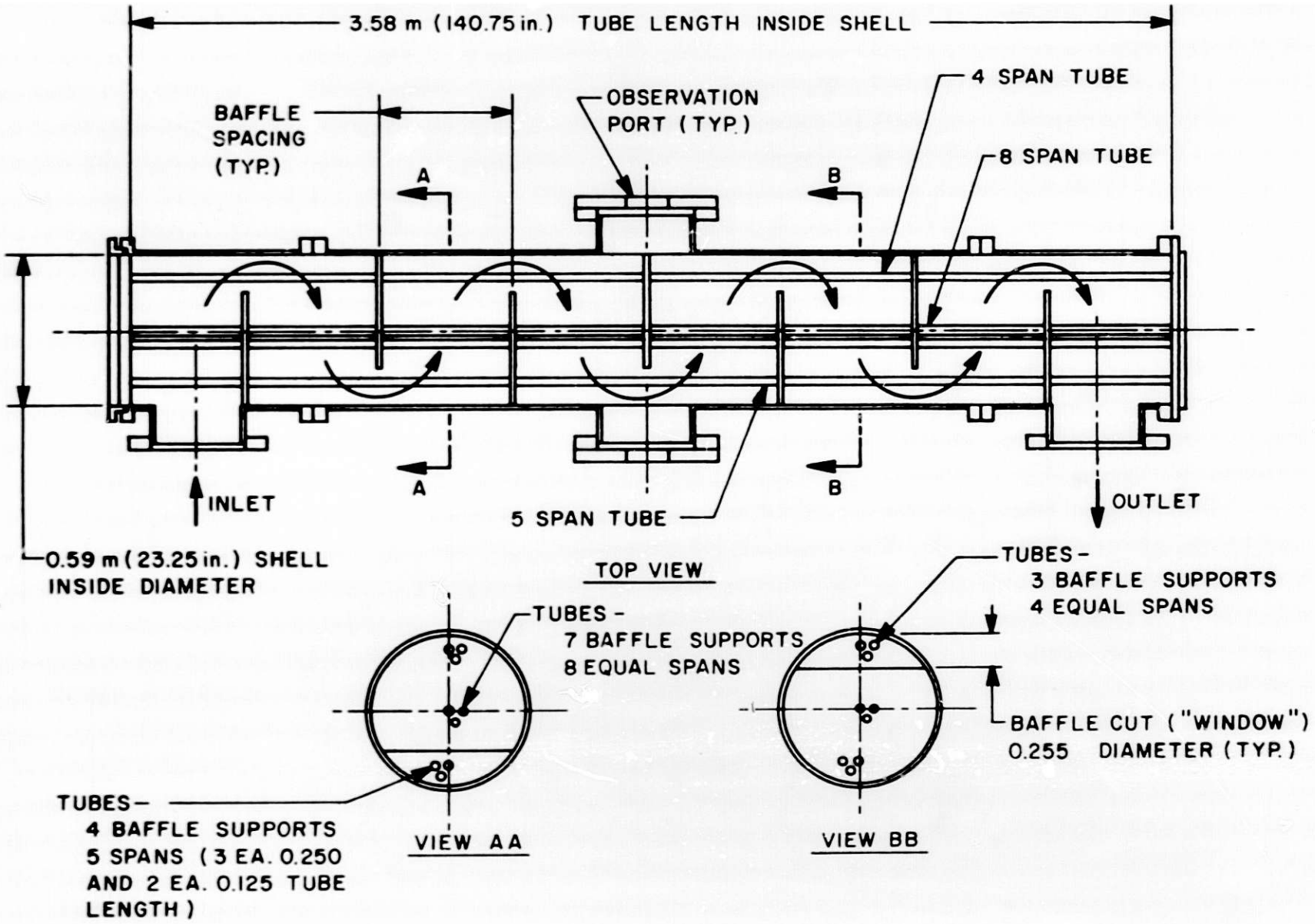

Configuration of Test Heat Exchanger
during initial tests

Fig. 5. Argonne test heat exchanger in seven-baffle/eight-crosspass configuration

Table 2. Description of Heat Exchanger

Shell:	
Length	3.58 m (140.75 in.)
Inside diameter	591 mm (23.25 in.)
Inlet/outlet nozzle, I.D.	337 mm (13.25 in.)
Baffles:	
Arrangement	7-Baffle/8-Crosspass
Thickness	9.5 mm (0.375 in.)
Outside diameter	587 mm (23.109 in.)
Baffle cut	29.8% of diameter (8-crosspass) 25.5% of diameter (6-crosspass)
Tube hole diameter	19.5 mm (0.768 in.)
Spacing (C to C)	447 mm (17.59 in.)
Tubes:	
Outside diameter	19.1 mm (0.750 in.)
Layout	Triangular (30° orientation)
Pitch-to-diameter	1.25
Radial Clearances:	
Tube-baffle	0.229 mm (0.009 in.)
Baffle-shell	1.79 mm (0.0705 in.)

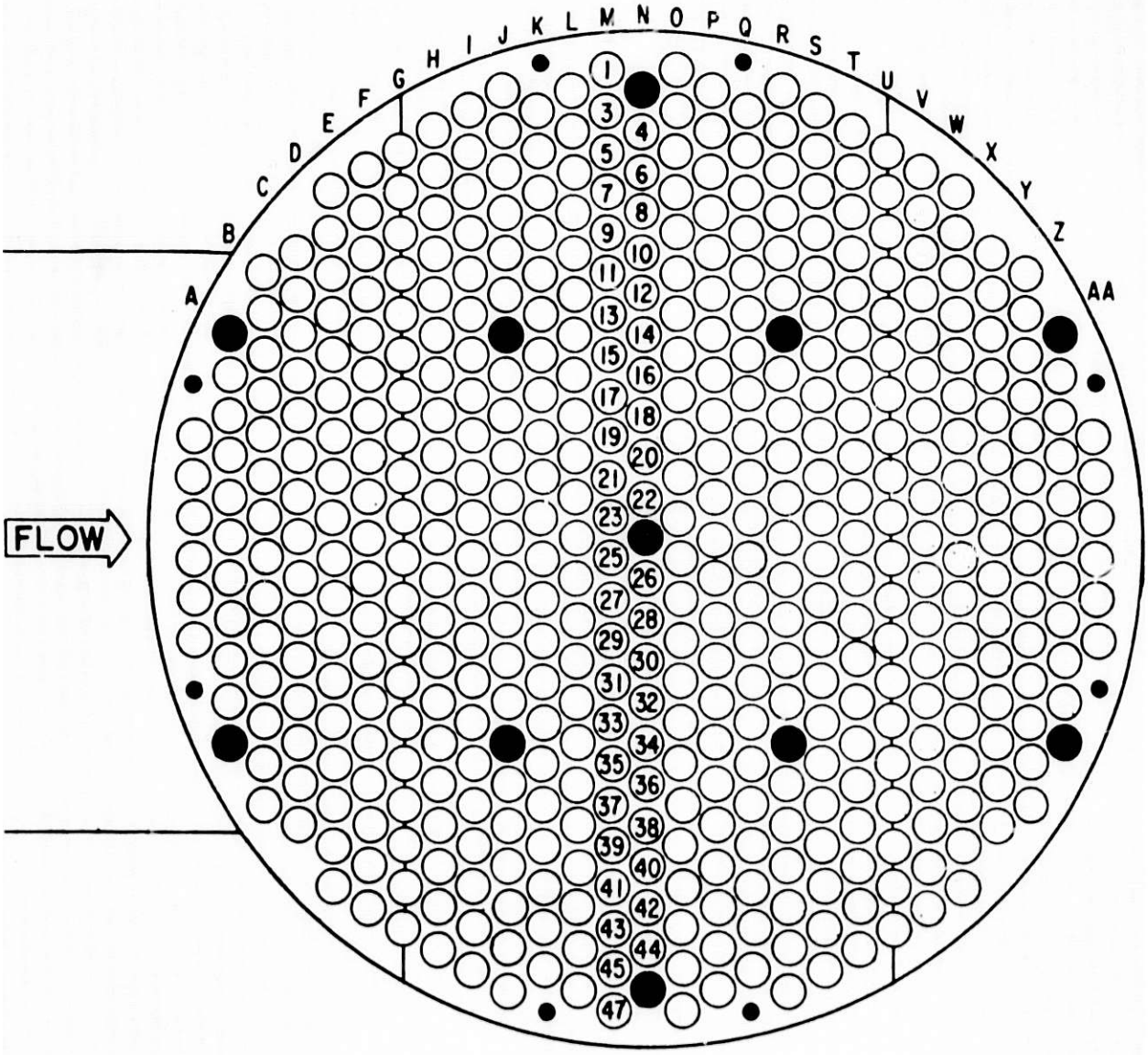

Fig. 6. Layout of heat exchanger tube bundle

"fictitious" cells be added around the perimeter of the original cell arrangement.

In the r-θ plane, twelve (12) angular divisions, each measuring 30°, were selected. The location of the baffle cut suggested the use of an even number of radial divisions; eight (8) radial divisions were chosen. The COMMIX-IHX/SG fictitious cell in the radial direction gives a total of nine (9) radial cells. A map of the cells in the r-θ plane is given in Fig. 3.

The seven-baffle, eight-crosspass configuration was chosen for the first simulation. For this configuration, the length of the heat exchanger is naturally partitioned into eight inter-baffle regions in the axial direction. To obtain a sufficiently detailed simulation of the flow, each such division must be again divided, preferably into four or more sections. Four axial divisions in each inter-baffle region were selected. Including one fictitious cell at each end, the heat exchanger has a total of thirty-four axial divisions as shown on the r-z map given in Fig. 7.

Hence, the computational mesh has 9, 12, and 34 cells as the maximum number of cells in the r-, θ-, and z-directions, respectively. This gives a total of 3,672 (3,072, if the fictitious cells are not included) computational cells for the numerical simulation. Each (r,θ,z) cell has dimensions of (1.453, π/6, 4.398) where the units are (inches, radians, inches). The cells are numbered from 1 to 9 radially, from 1 to 12 azimuthally (clockwise, in clock-number positions), and from 1 to 34 axially (from inlet to outlet).

It should be noted that, given the symmetry of the heat exchanger configuration under consideration, it would have been quite reasonable to consider only one-half of the unit in the simulation; a cross section through the shell, parallel to the z-axis, is symmetric about a plane through the centerline of the inlet/outlet nozzles (see Fig. 3). However, for the initial test runs the symmetrical situation was not taken advantage of.

C. COMMIX-IHX/SG Input/Output

To produce a numerical simulation, the COMMIX-IHX/SG code requires specifications for two sets of input data. The first set includes variables describing the size and number of computational cells, the number of iterations and timesteps to be performed, and the information to be displayed as written or taped output. The second set of data contains supplementary values which are used to give a description of the internal layout of the heat exchanger.

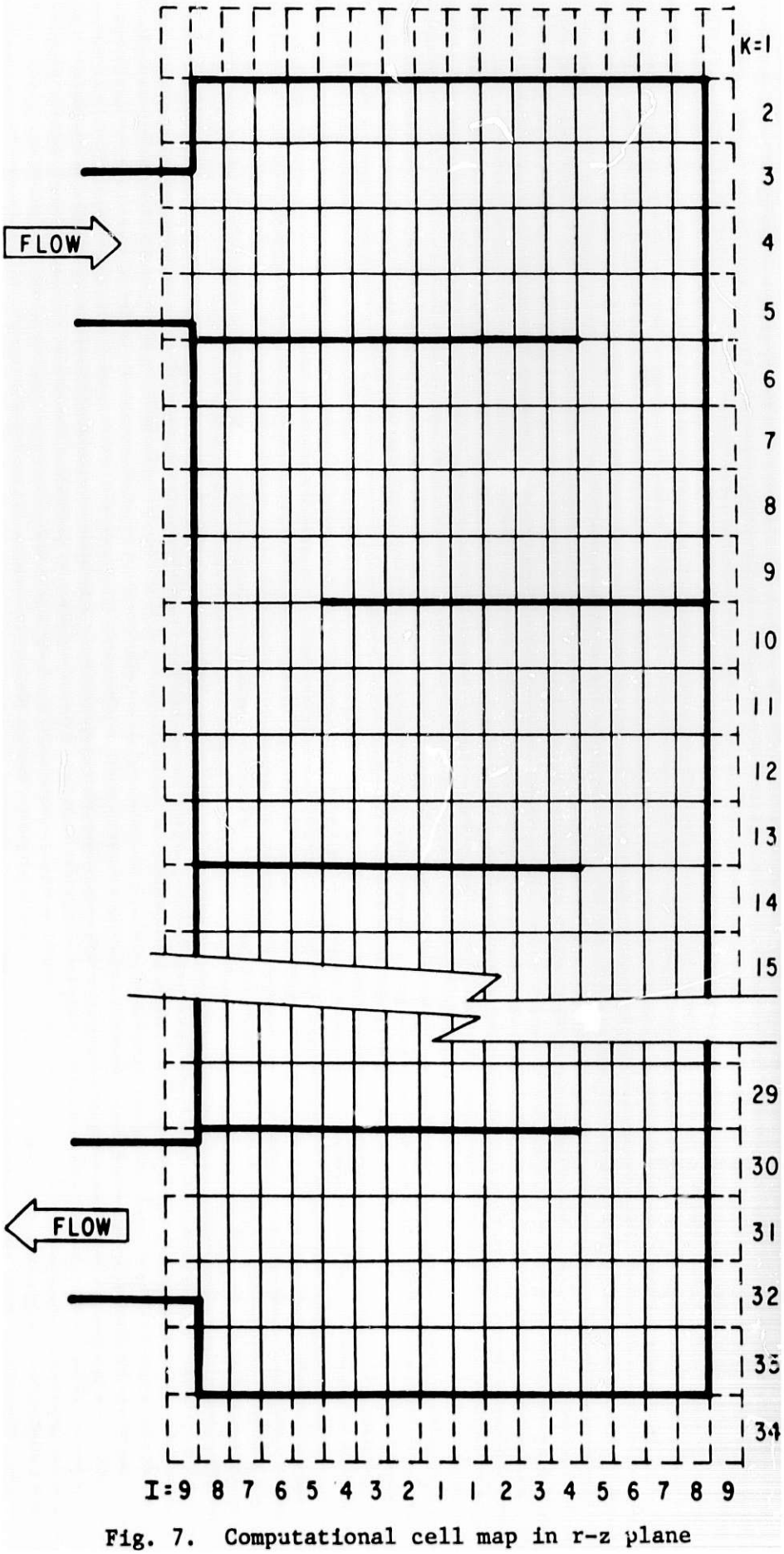

Fig. 7. Computational cell map in r-z plane

The output of COMMIX-IHX includes a tabular listing of u-, v-, and w-components of flow velocity for each computational cell. Sample output giving the u and v velocities for cells (I,J,6) is given in Table 3. Computer graphics are also available to generate plots of flow distribution for selected cross-sections through the unit. As examples, the flow pattern in the r-z plane at J-section 3-9 (a cross-section through the centerline of the inlet/outlet nozzles) is given in Fig. 8 and patterns in the r-θ plane at z-positions K = 3 and 5 and are given in Figs. 9 and 10, respectively. Figures 8-10 serve to illustrate the three-dimensional, nonuniform nature of the flow. At this time, no experimental measurements of flow distribution are available from the vibration tests for use in evaluating the code predictions.

D. Vibration Analysis

A post processor type program was written to implement the prediction method outlined in Section III. In summary, the post-processor uses the computational cell flow velocities computed by COMMIX-IHX/SG as input and, for each tube within the exchanger, computes (1) V(z) according to Eq. (8), using linear interpolation to obtain u_T and v_T; (2) the ratio u/v; (3) $\phi_n(z)$ using the BEAMINT code; and (4) U_{en} according to Eq. (5). The magnitude of V(z) is both printed out and plotted, as illustrated in Figs. 11 and 12 for tubes V-24 and X-24, respectively. The magnitude is taken as positive or negative in accordance with the sign associated with the u-component of velocity. The ratio u/v is also printed (see Figs. 11 and 12). In Fig. 13 a smooth curve is drawn through the data points for tube V-24. The curve in Fig. 13 clearly depicts the nonuniformity of the crossflow velocity distribution over the tube.

The tube vibration modes for the first six (6) modes of the 4- and 5-span tubes in the window regions of the seven-baffle/eight-crosspass heat exchanger are given in Fig. 14, as determined with the BEAMINT code. Because the velocity distribution is different for each tube, each tube will have a different effective flow velocity corresponding to each of its mode shapes. Values of the effective velocity are computed for the first eight vibration modes and are printed out as shown in the table at the top of Figs. 11 and 12.

Knowing the effective crossflow velocities for the various vibration mode shapes, the reduced effective crossflow velocities are computed as

$$\bar{U}_n = \frac{U_{en}}{f_n d} \; ; \tag{9}$$

sample results are given in Table 4. A map of the maximum value of the reduced effective crossflow velocities for the tubes in the window regions

Table 3. Sample Output: u and v Velocities for Cells (I,J,6)

u-Component of Shellside Flow Velocity (m/s)

K = 6

I--> / J	1	2	3	4	5	6	7	8	9
12	2.539E-02	4.672E-02	5.892E-02	4.610E-02	3.455E-03	7.117E-03	-6.997E-03	0.0	0.0
11	3.676E-03	4.143E-02	6.982E-02	7.636E-02	6.399E-02	5.360E-02	2.726E-02	0.0	0.0
10	2.371E-02	7.228E-02	9.582E-02	9.228E-02	7.230E-02	4.819E-02	2.176E-02	0.0	0.0
9	2.370E-02	7.227E-02	9.579E-02	9.225E-02	7.228E-02	4.818E-02	2.175E-02	0.0	0.0
8	3.675E-03	4.142E-02	6.980E-02	7.634E-02	6.398E-02	5.359E-02	2.725E-02	0.0	0.0
7	2.539E-02	4.671E-02	5.891E-02	4.609E-02	3.454E-03	7.115E-03	-6.995E-03	0.0	0.0
6	4.819E-02	4.573E-02	2.011E-02	-2.093E-02	-5.296E-02	-1.328E-02	-2.193E-02	0.0	0.0
5	3.864E-02	-2.105E-03	-1.702E-01	-5.359E-01	-3.160E-01	-6.090E-01	-3.130E-01	0.0	0.0
4	-6.428E-02	-1.248E-01	-2.286E-01	-5.534E-01	-1.029E-01	1.345E-01	7.003E-02	0.0	0.0
3	-6.430E-02	-1.248E-01	-2.286E-01	-5.536E-01	-1.029E-01	1.346E-01	7.005E-02	0.0	0.0
2	3.865E-02	-2.105E-03	-1.703E-01	-5.361E-01	-3.161E-01	-6.091E-01	-3.131E-01	0.0	0.0
1	4.820E-02	4.574E-02	2.012E-02	-2.094E-02	-5.297E-02	-1.329E-02	-2.194E-02	0.0	0.0

v-component of Shellside Flow Velocity (m/s)

K = 6

I--> / J	1	2	3	4	5	6	7	8	9
12	3.064E-02	3.467E-02	2.011E-02	2.415E-02	5.763E-02	-3.841E-02	2.495E-02	3.638E-02	-3.6 8E-02
11	4.444E-02	2.806E-02	3.112E-03	-5.501E-03	-7.432E-03	-4.005E-02	-4.641E-02	-4.257E-02	4.2 7E-02
10	3.824E-02	1.998E-02	7.061E-03	.315E-03	1.073E-02	8.178E-03	7.562E-03	4.109E-03	-4.109E-03
9	-3.160E-02	-2.723E-02	-2.344E-02	-2.054E-02	-1.860E-02	-1.723E-02	-1.595E-02	-1.626E-02	1.626E-02
8	-3.825E-02	-1.999E-02	-7.063E-03	-7.317E-03	-1.073E-02	-8.180E-03	-7.564E-03	-4.110E-03	4.110E-03
7	-4.445E-02	-2.806E-02	-3.113E-03	5.503E-03	7.434E-03	4.006E-02	4.643E-02	4.258E-02	-4.2 8E-02
6	-3.065E-02	-3.468E-02	-2.012E-02	-2.416E-02	-5.764E-02	3.842E-02	-2.495E-02	-3.639E-02	3.6 9E-02
5	4.103E-03	-2.915E-02	-4.177E-02	9.437E-03	2.076E-01	4.155E-01	4.806E-01	5.289E-01	-5.289E-01
4	3.929E-02	-5.930E-03	-1.195E-01	-1.742E-01	-1.276E-01	-4.992E-01	2.834E-01	6.556E-01	-6.5 6E-01
3	2.798E-02	1.148E-02	-5.292E-03	-3.055E-02	-5.066E-02	-1.216E-01	-4.419E-02	2.308E-01	-2.308E-01
2	-3.928E-02	5.929E-03	1.194E-01	1.742E-01	1.275E-01	4.990E-01	-2.833E-01	-6.554E-01	6.5 4E-01
1	-4.102E-03	2.914E-02	4.176E-02	-9.435E-03	-2.076E-01	-4.154E-01	-4.805E-01	-5.288E-01	5.288E-01

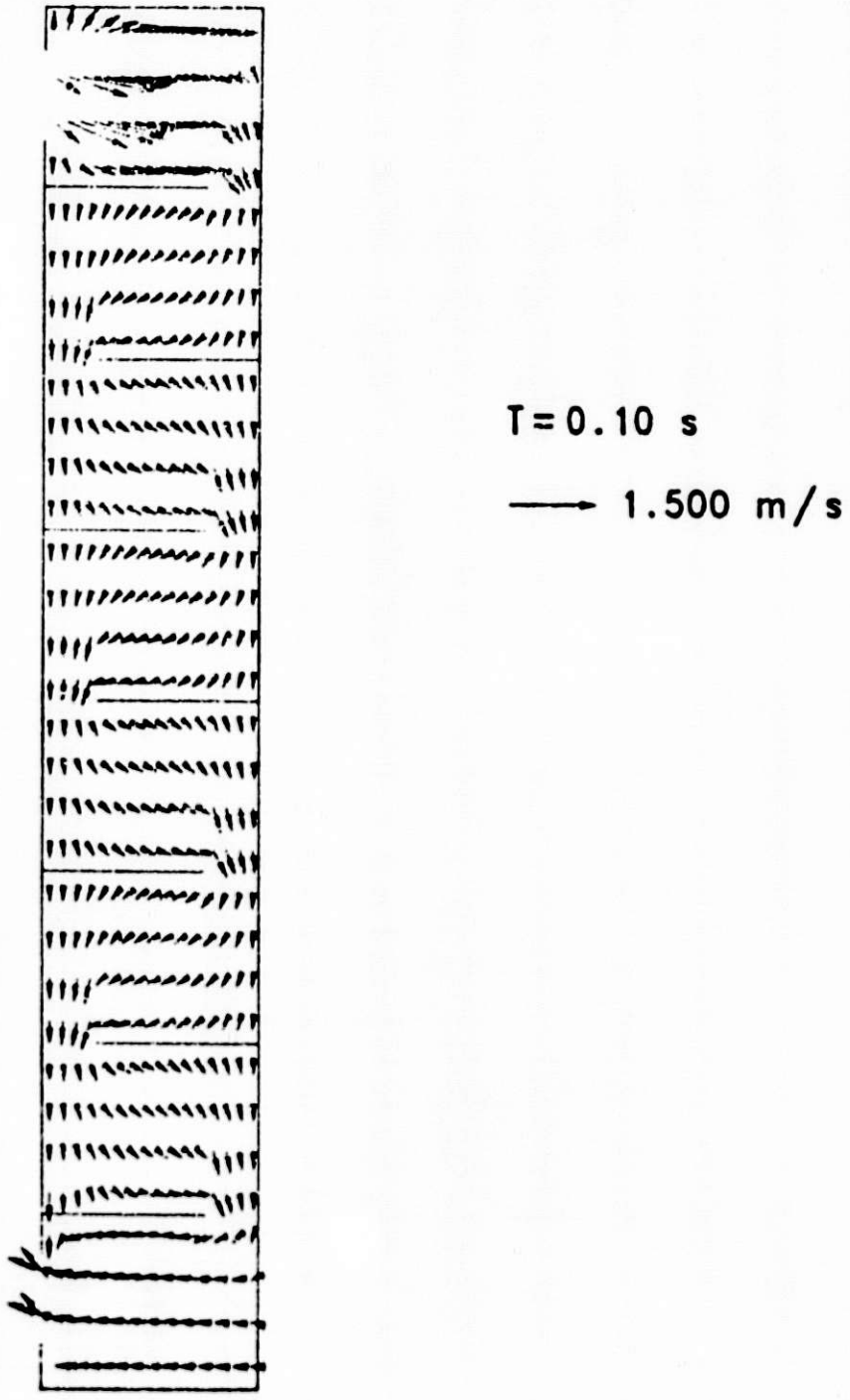

Fig. 8. Flow pattern in r-z plane at J-section 3-9 (a cross-section through the centerline of the inlet/outlet nozzle)

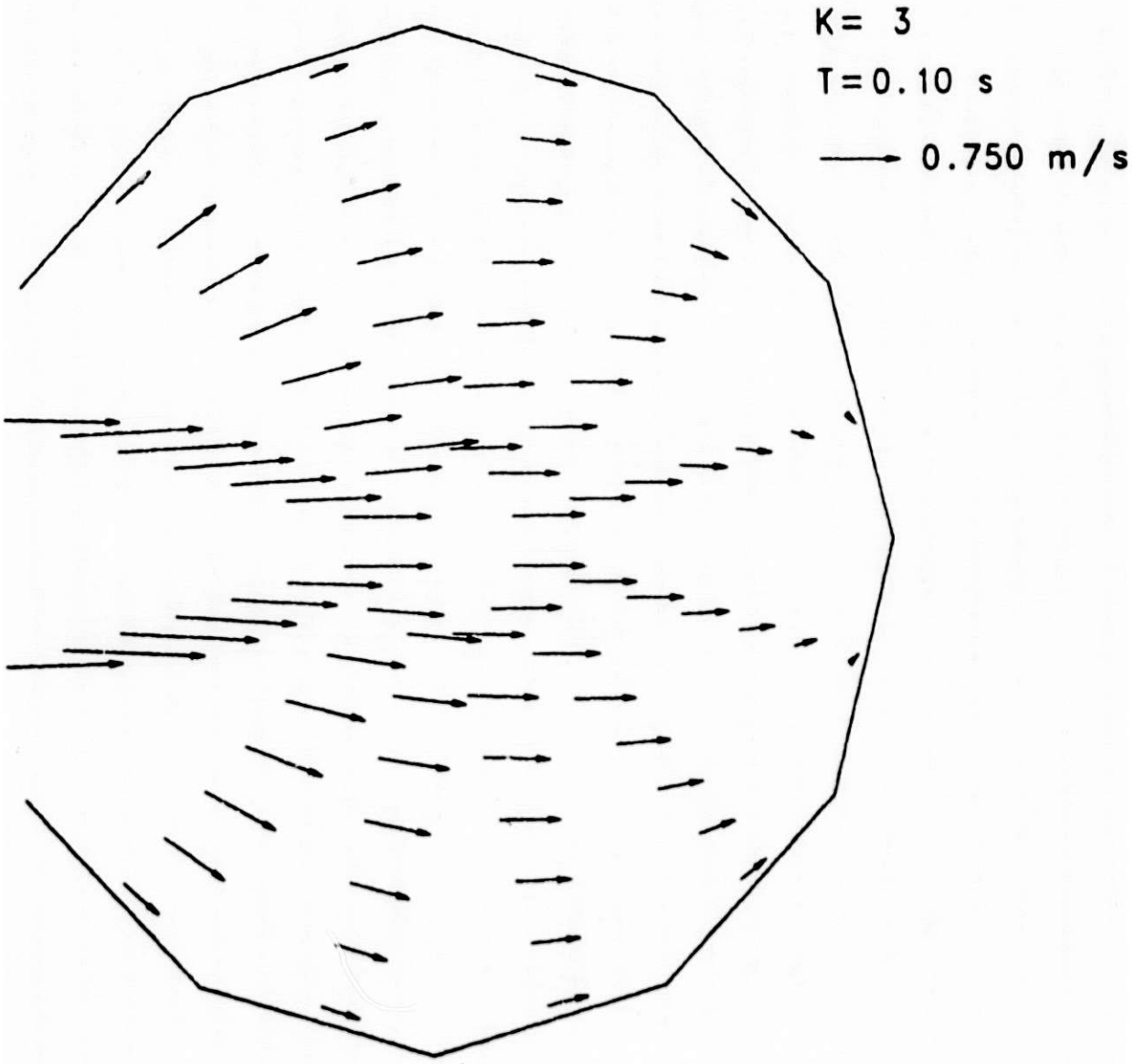

Fig. 9. Flow pattern in r-θ plane at axial location K = 3

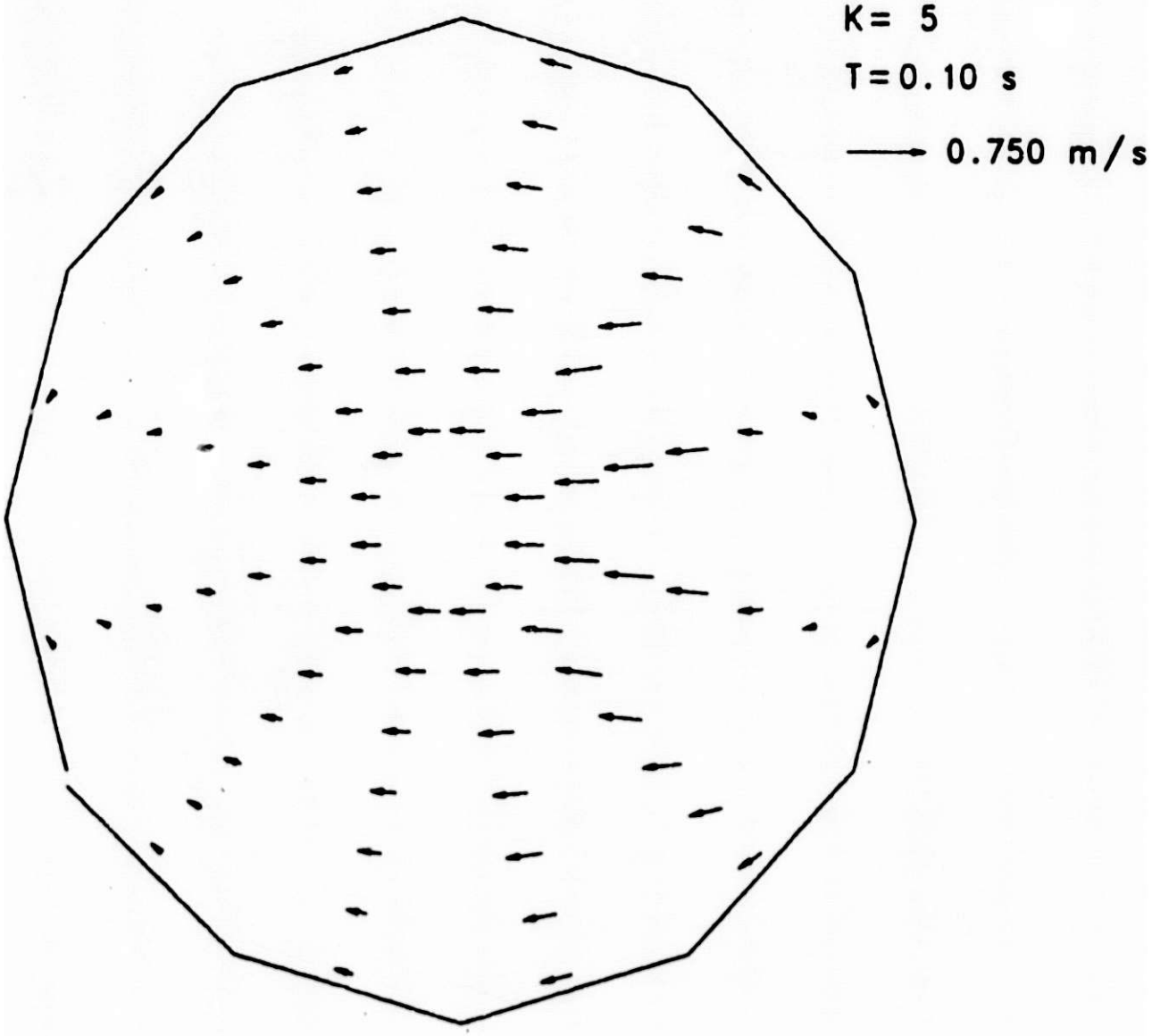

Fig. 10. Flow pattern in r-θ plane at axial location K = 5

```
 THIS IS THE VELOCITY DISTRIBUTION FOR FLOW PAST 2 TUBES IN THE    4-SPAN WINDOW. THE TUBES ARE LABELLED
TUBES V     24 AND  24.THE EFFECTIVE VELOCITIES ARE( M/S)

          1.5560 FOR MODE 1
          1.7113 FOR MODE 2
          1.9464 FOR MODE 3
          1.8854 FOR MODE 4
          1.2985 FOR MODE 5
          1.4907 FOR MODE 6
          1.5753 FOR MODE 7
          1.3762 FOR MODE 8

                                                THE GRAPH VELOCITY IS IN METERS / SECOND.

|U / V|    FLOW -6.0     -5.0     -4.0     -3.0     -2.0     -1.0      0.0      1.0      2.0      3.0      4.0      5.0      6.0

-.333E+03  1.5514                                                      +----------*
-.243E+03  2.2399                                                      +----------------*
-.156E+03  2.2661                                                      +----------------*
-.740E+02  4.1548                                                      +--------------------------------*
                  :::::::::::::::::::::::::::::::::::::::::: BAFFLE  :>>
0.701E+01 -0.3546                                                        *--+
0.117E+02 -0.7912                                                     *------+
0.250E+02 -1.1486                                                    *---------+
0.613E+02 -1.7345                                              *---------------+
                  :::::::::::::::::::::::::::::::::::::::::::::::::::: BAFFLE  ::::::::::::::::::::::::::::::::::::::::::::::::::::
-.950E+01  0.1766                                                      +-*
-.181E+02  0.4198                                                      +---*
-.221E+02  0.6653                                                      +-----*
-.230E+02  2.5507                                                      +----------------------*
                  :::::::::::::::::::::::::::::::::::::::::: BAFFLE  :>>
0.162E+02 -0.9593                                                        *---------+
0.199E+02 -1.1676                                                     *----------+
0.393E+02 -1.2341                                                     *----------+
0.133E+03 -1.5525                                              *-------------+
                  :::::::::::::::::::::::::::::::::::::::::::::::::::: BAFFLE  ::::::::::::::::::::::::::::::::::::::::::::::::::::
-.960E+01  0.1720                                                      +-*
-.179E+02  0.4102                                                      +---*
-.217E+02  0.6537                                                      +-----*
-.228E+02  2.5433                                                      +----------------------*
                  :::::::::::::::::::::::::::::::::::::::::: BAFFLE  :>>
0.165E+02 -0.9721                                                        *---------+
0.201E+02 -1.1802                                                     *----------+
0.395E+02 -1.2448                                                     *----------+
0.130E+03 -1.5607                                              *-------------+
                  :::::::::::::::::::::::::::::::::::::::::::::::::::: BAFFLE  ::::::::::::::::::::::::::::::::::::::::::::::::::::
-.793E+01  0.1617                                                      +*
-.144E+02  0.3879                                                      +--*
-.164E+02  0.6032                                                      +----*
-.171E+02  2.5525                                                      +----------------------*
                  :::::::::::::::::::::::::::::::::::::::::: BAFFLE  :>>
0.139E+02 -1.0870                                                        *----------+
0.184E+02 -1.3748                                                     *------------+
0.350E+02 -1.4509                                                     *------------+
0.975E+02 -1.5089                                              *-------------+
```

Fig. 11. Computer output for resultant crossflow velocity distribution for flow past tube V-24

```
 THIS IS THE VELOCITY DISTRIBUTION FOR FLOW PAST 2 TUBES IN THE    4-SPAN WINDOW. THE TUBES ARE LABELLED
TUBES Z     24 AND  24.THE EFFECTIVE VELOCITIES ARE( M/S)

          0.5852 FOR MODE 1
          0.6807 FOR MODE 2
          0.8074 FOR MODE 3
          0.7568 FOR MODE 4
          0.5221 FOR MODE 5
          0.6028 FOR MODE 6
          0.6267 FOR MODE 7
          0.5348 FOR MODE 8

                                                THE GRAPH VELOCITY IS IN METERS / SECOND.

|U / V|    FLOW -6.0      -5.0      -4.0      -3.0      -2.0      -1.0       0.0       1.0       2.0       3.0       4.0       5.0       6.0

-.118E+03  0.5128                                                            +----*
-.303E+03  0.8466                                                            +-------*
0.124E+03  0.7557                                                            +------*
0.145E+02  1.9330                                                            +----------------*
                  :::::::::::::::::::::::::::::::::::::::::: BAFFLE  :>>
0.673E+01  0.0823                                                            +*
0.155E+02 -0.3514                                                          *--+
0.134E+02 -0.5280                                                        *----+
0.183E+02 -0.7612                                                      *------+
                  :::::::::::::::::::::::::::::::::::::::::::::::::: BAFFLE  ::::::::::::::::::::::::::::::::::::::::::::::::::
-.390E+01  0.0640                                                            +*
-.888E+01  0.1517                                                            +*
-.146E+02  0.1976                                                            +-*
0.435E+01  0.9376                                                            +-------*
                  :::::::::::::::::::::::::::::::::::::::::: BAFFLE  :>>
-.113E+03 -0.2654                                                          *--+
0.127E+02 -0.4710                                                        *----+
0.145E+02 -0.5132                                                        *----+
0.293E+02 -0.6304                                                      *------+
                  :::::::::::::::::::::::::::::::::::::::::::::::::: BAFFLE  ::::::::::::::::::::::::::::::::::::::::::::::::::
-.425E+01  0.0661                                                            +*
-.905E+01  0.1502                                                            +*
-.144E+02  0.1942                                                            +-*
0.434E+01  0.9371                                                            +-------*
                  :::::::::::::::::::::::::::::::::::::::::: BAFFLE  :>>
-.977E+02 -0.2695                                                          *--+
0.122E+02 -0.4750                                                        *----+
0.146E+02 -0.5166                                                        *----+
0.289E+02 -0.6330                                                      *------+
                  :::::::::::::::::::::::::::::::::::::::::::::::::: BAFFLE  ::::::::::::::::::::::::::::::::::::::::::::::::::
-.349E+01  0.0625                                                            +*
-.692E+01  0.1386                                                            +*
-.830E+01  0.1544                                                            +*
0.343E+01  0.9171                                                            +-------*
                  :::::::::::::::::::::::::::::::::::::::::: BAFFLE  :>>
-.266E+02 -0.3224                                                          *--+
0.144E+02 -0.5503                                                        *----+
0.146E+02 -0.5986                                                        *----+
0.245E+02 -0.6344                                                      *------+
```

Fig. 12. Computer output for resultant crossflow velocity distribution for flow past tube Z-24

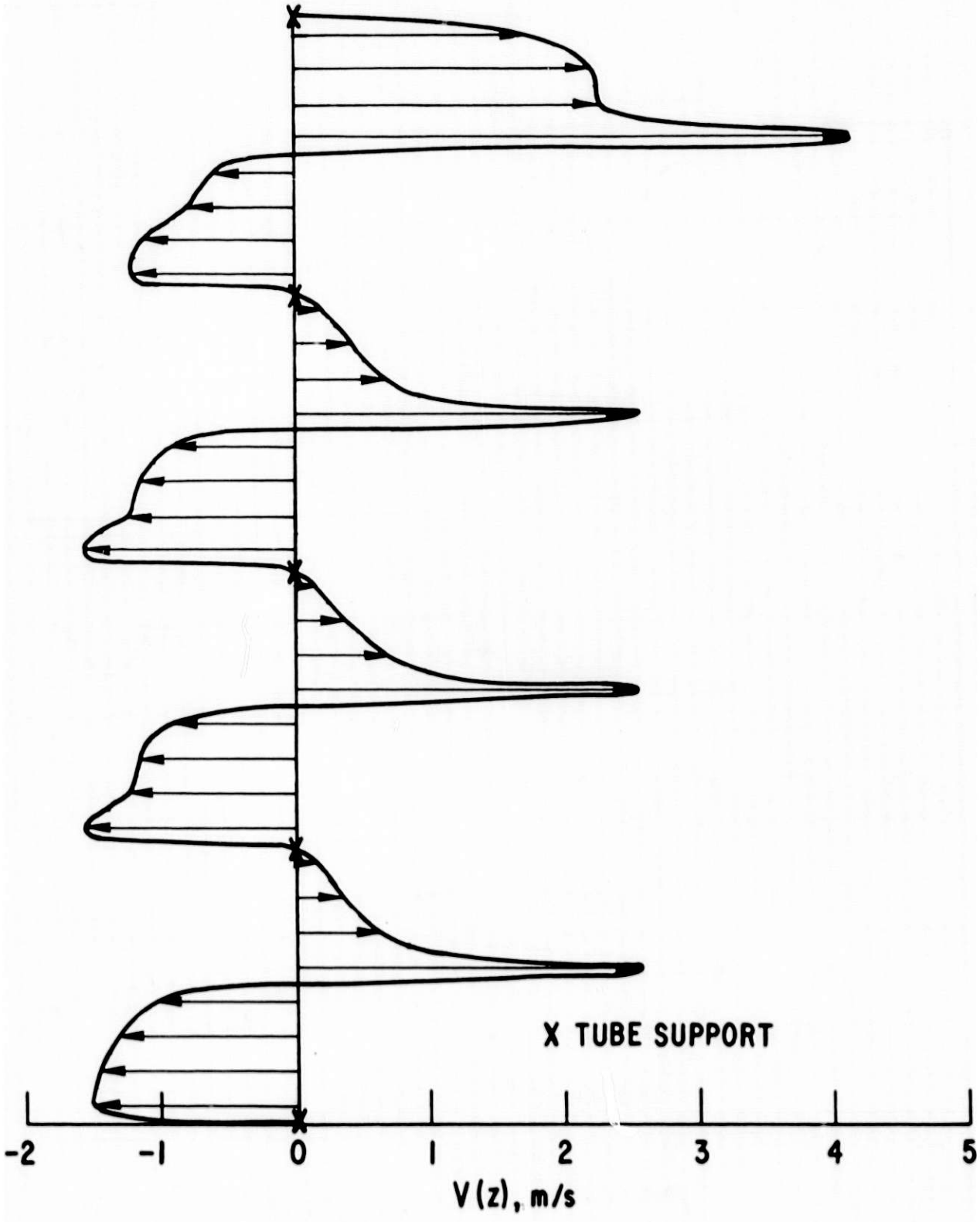

Fig. 13. Resultant crossflow velocity distribution for flow past tube V-24

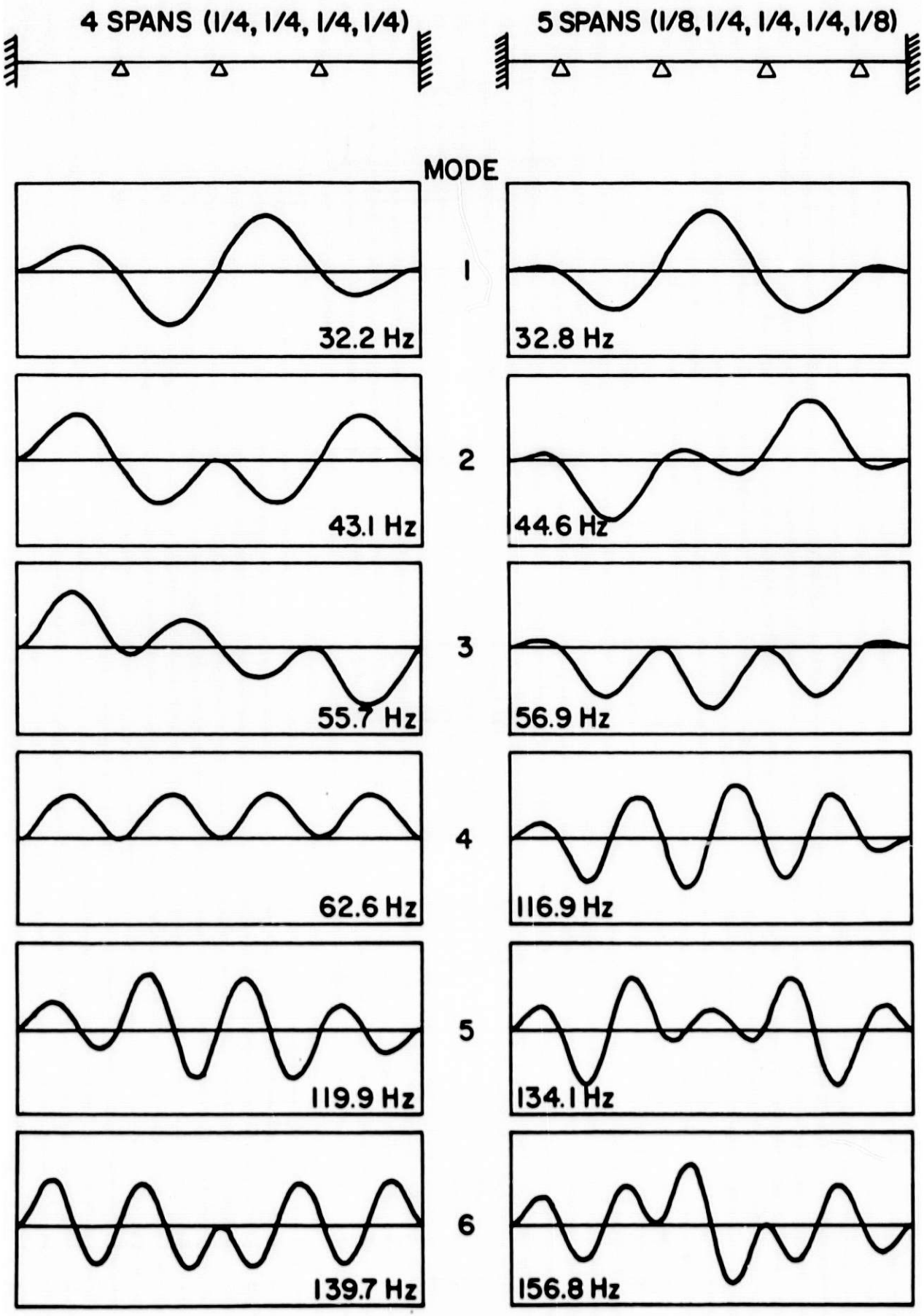

Fig. 14. Theoretical tube vibration mode shapes and frequencies, with water on shellside; n = 1-6

Table 4. Sample Results: Reduced Effective Crossflow Velocities ($\bar{U}_n$) - 7-Baffle Configuration, Q = 0.208 m^3/s (3,300 gpm)

n	A-23/25	B-24	C-23/25	D-24	E-23/25
1	0.40	0.67	0.89	1.28	1.29
2	0.30	0.50	0.66	0.93	0.94
3	0.21	0.36	0.49	0.68	0.70
4	0.16	0.28	0.34	0.53	0.50
5	0.15	0.26	0.31	0.47	0.45
6	0.12	0.21	0.26	0.40	0.38

n	F-24	V-24	W-23/25	X-24	Y-23/25
1	1.74	2.54	2.14	1.82	1.45
2	1.27	2.08	1.77	1.53	1.24
3	0.92	1.83	1.57	1.38	1.13
4	0.71	1.58	1.35	1.17	0.95
5	0.64	0.57	0.49	0.42	0.34
6	0.53	0.56	0.48	0.41	0.34

n	Z-24	AA-23/25	V-6/42	X-16/32	C-19/29
1	0.95	0.65	2.34	1.65	1.01
2	0.83	0.54	1.68	1.32	0.74
3	0.76	0.48	1.23	1.12	0.54
4	0.63	0.41	1.20	0.98	0.41
5	0.23	0.13	0.39	0.35	0.37
6	0.23	0.13	0.34	0.34	0.31

is given in Fig. 15; taking advantage of the symmetry of the tube bundle, only one-half of the exchanger is shown. For the particular configuration simulated, the maxima correspond to the first vibration mode. This will not be true in general.

V. EVALUATION OF RESULTS

The prediction method was applied to both a seven-baffle/eight-crosspass and a five-baffle/six-crosspass full tube bundle configuration. The volumetric flow rate simulated was 3,300 gpm for the seven-baffle case and 2,000 gpm for the five-baffle case. Results in the form of a map of the maximum value of the reduced effective crossflow velocities are given in Fig. 15 for the seven-baffle configuration, and in Fig. 16 for the five-baffle configuration. It is reasonable to assume that the mass-damping parameter, δ_m in Table 1, is approximately the same for each tube. With this assumption, the tubes with the highest values of reduced effective flow velocity would be expected to experience instability first and to vibrate with the largest amplitude.

A. Qualitative Comparison with Experimental Results

Evaluation of the results obtained by the subject prediction method can be made by comparison with the experimental results from the Argonne test heat exchanger [5,7].

During flow testing of the seven-baffle configuration, at instability, which initiated in the range 3,130 to 3,250 gpm, more than 25 tubes were shaken severely enough to slide and move axially in their O-ring seals, thereby providing a reasonably good indication where the most severe "action" took place [5]. As shown in Fig. 17, the tubes most strongly subjected to the instability were located in the far window region (a) in rows V and W next to the row saddled in the baffle cut, and (b) in the regions where the baffle cut meets the shell. As the flow rate was increased further, in the range of 3,430 to 3,760 gpm, tubes in the near window region also experienced high level vibration with tube F-22, as indicated in Fig. 17, vibrating violently enough to move axially.

In Fig. 18, the tubes in the far window region (4-span tubes) with a computed reduced effective crossflow velocity greater than 2.00, as obtained from the data given in Fig. 15, are indicated by shading as are those tubes in the near window region with a reduced effective crossflow velocity greater than 1.70. A comparison between Figs. 17 and 18 shows excellent agreement between those tubes with high values of reduced effective flow velocity and tubes that experienced high levels of instability.

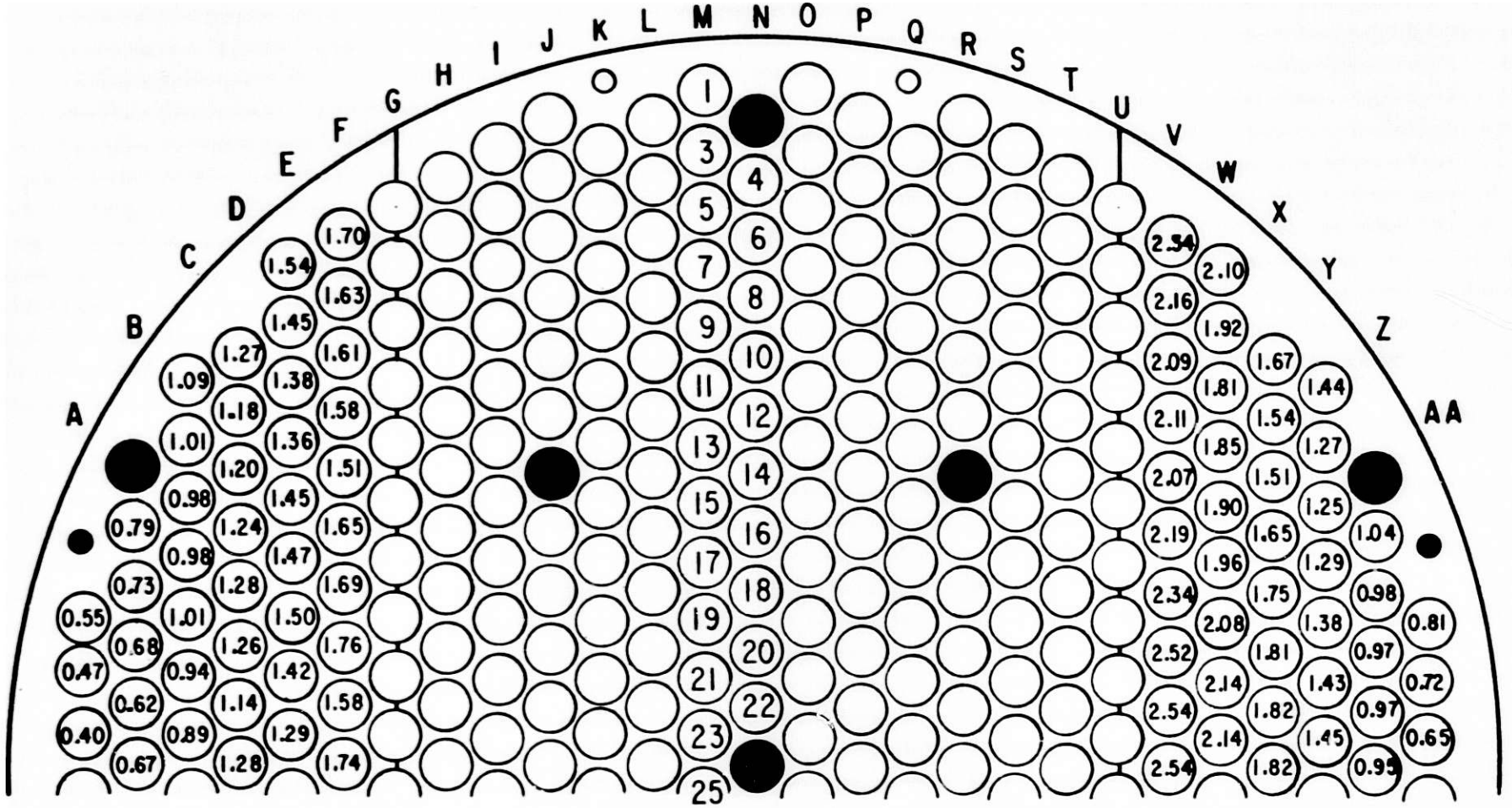

Fig. 15. Reduced effective flow velocities for tubes in window regions; 7-baffle configuration, Q = 3,300 gpm

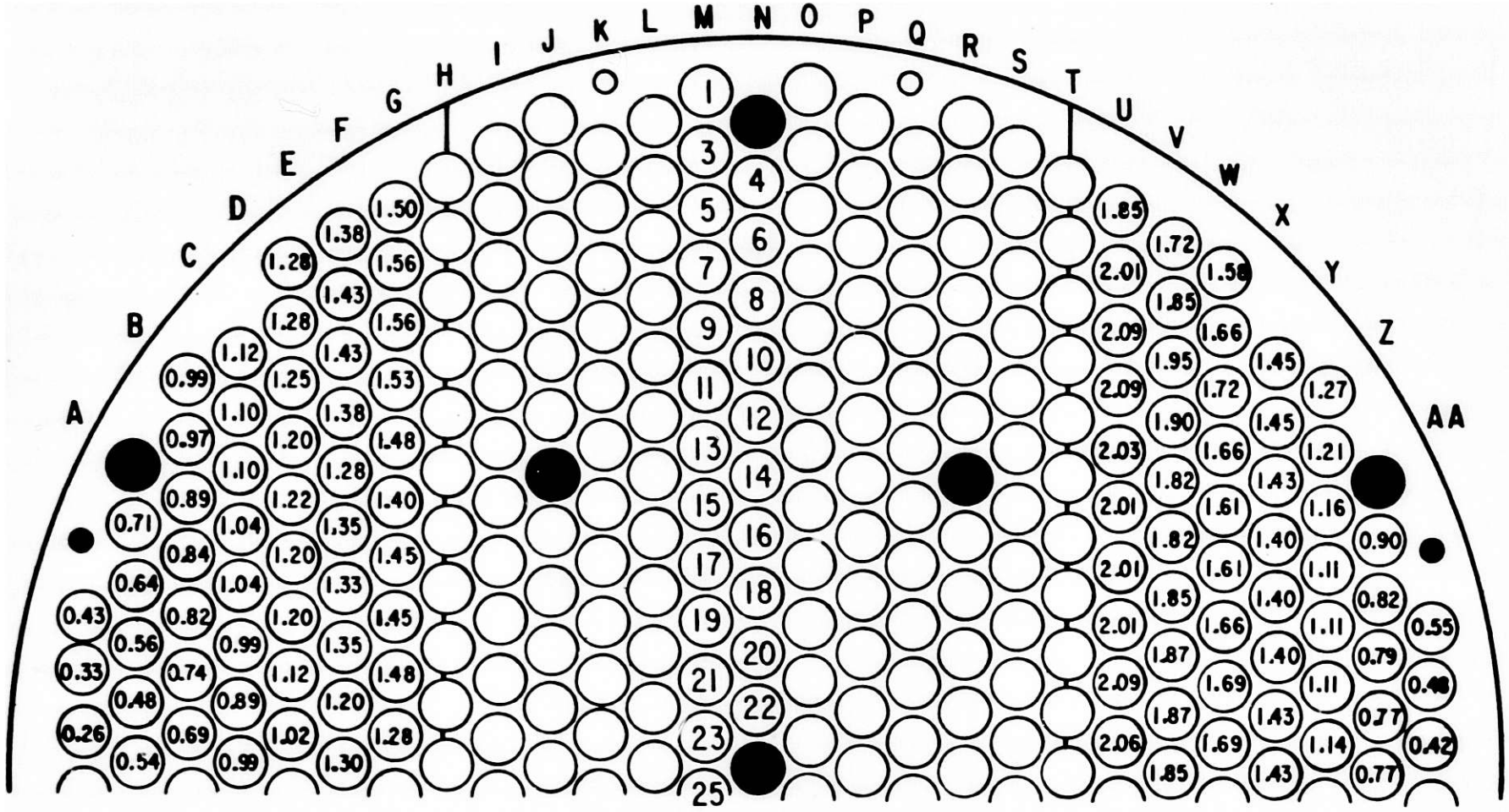

Fig. 16. Reduced effective flow velocities for tubes in window regions; 5-baffle configuration, Q = 2,000 gpm

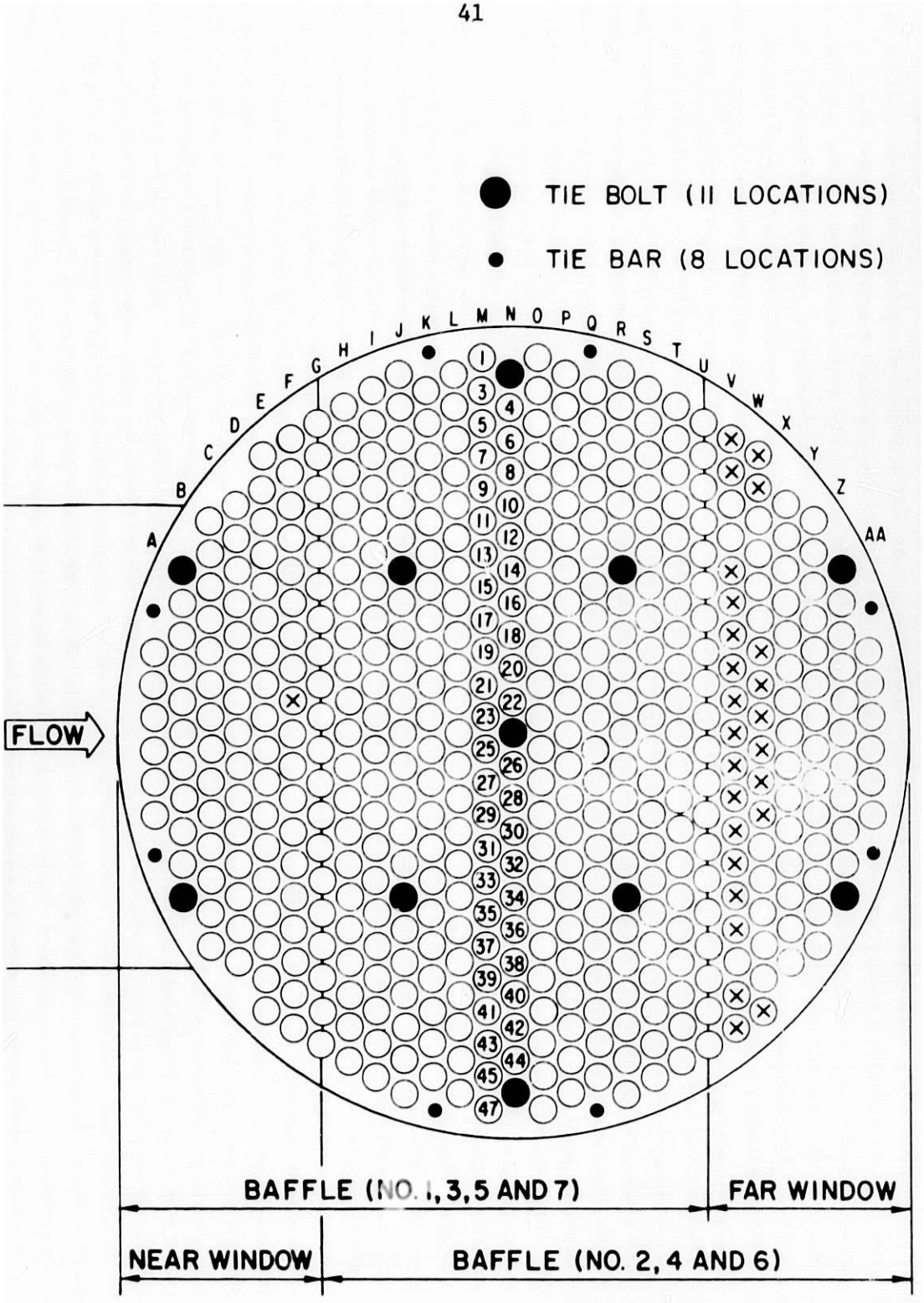

Fig. 17. Experimental data from tube vibration test [5]: ⊗ - tube with large amplitude vibration; 7-baffle configuration

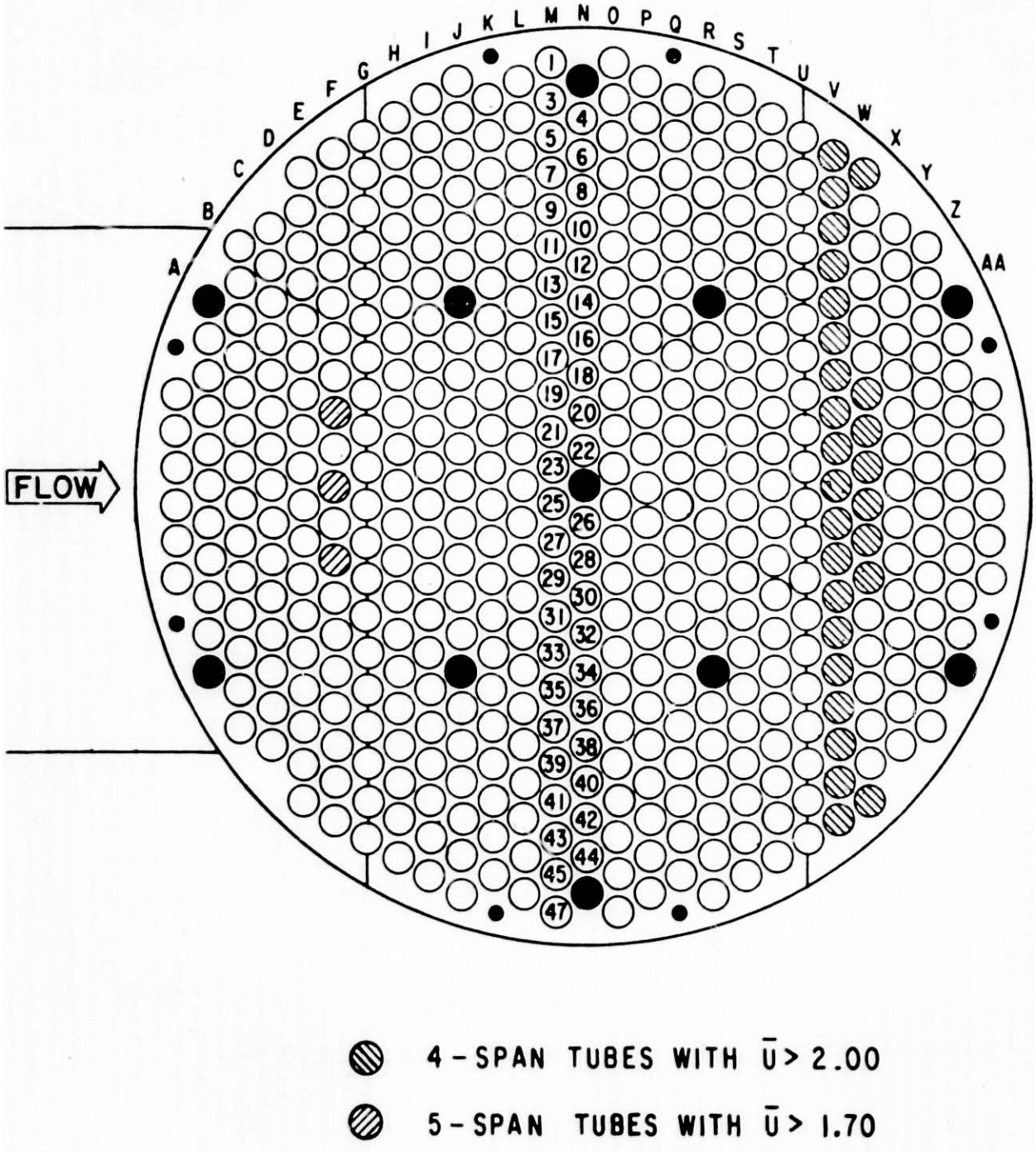

Fig. 18. Tubes with high values of reduced effective flow velocities; 7-baffle configuration, Q = 3,300 gpm

Dynamic behavior of the five-baffle/six-crosspass, full-bundle configuration is described as follows [7]:

> "... The tubes most susceptible to instability were located in the central region of tube rows U and V adjacent to the baffle edge in the far window region opposite the nozzles. There the onset of instability occurred in the range of 1980 to 2140 gal/min.... In the 'near' window, on the side of the nozzles, substantial tube vibration began at the higher flowrates, particularly in the row next to the baffle cut where tube-to-tube impact occurred. However, no significant excitation of the row A tubes immediately exposed to the flow emerging from the nozzle was observed."

Instability in the near window initiated at a flow rate of approximately 2,790 to 3,000 gpm.

In Fig. 19, the tubes in the far window region (3-span tubes) with a computed reduced effective crossflow velocity greater than or equal to 1.85, as obtained from the data given in Fig. 16, are indicated by shading as are those tubes in the near window region with a reduced effective crossflow velocity greater than or equal to 1.45. The selection of 1.85 and 1.45 as threshold values is, of course, somewhat arbitrary. Nevertheless, there is, again, excellent qualitative agreement with the observed dynamic behavior of the tube bundle.

It is encouraging that the simulation correctly predicts the tubes in the first two rows past the baffle cut in the far window region to be most susceptible to fluidelastic excitation by virtue of their high reduced effective crossflow velocities. This result agrees with experiment, as discussed above, and also with industrial practice relative to a field fix which involves removing the row of tubes adjacent to the baffle cut as a means to reduce the potential for tube bundle vibration in a given unit. However, it is equally significant that the simulation correctly predicts, in both cases, that the tubes directly exposed to the incoming flow from the inlet nozzle, viz., tubes in rows A and B, have a low potential for fluidelastic excitation. Intuitively one might expect this group of tubes to be susceptible to vibration. In fact, in the heat exchanger test program, tube A-23 was one of the tubes selected to be instrumented in the initial series of flow tests; however, test results indicated relatively low level vibrations throughout the range of flow rates tested. Further agreement is provided by the fact that the tubes in the near window region with the highest values of reduced effective crossflow velocity (adjacent to baffle edge) are from the same general grouping of tubes that experiences high level vibration caused by fluidelastic excitation in the water flow tests.

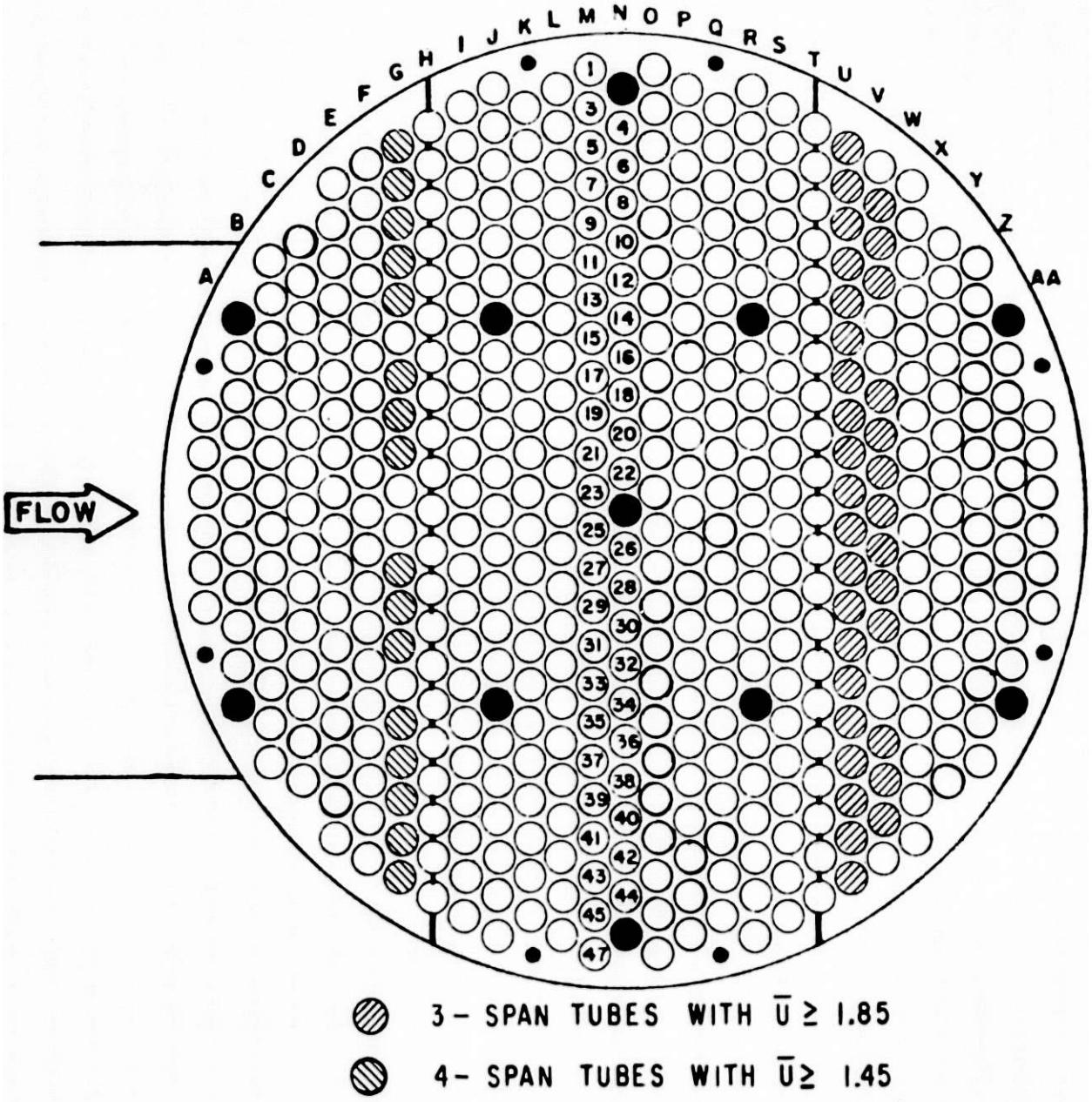

Fig. 19. Tubes with high values of reduced effective flow velocities; 5-baffle configuration, Q = 2,000 gpm

B. Quantitative Comparison with Laboratory Results and Design Guides

It has been shown in the previous subsection that qualitatively there is excellent agreement between predicted and experimental results in the sense that tubes with the highest predicted value of reduced effective crossflow velocity correspond to the general groupings of tubes that first experience instability in the water flow tests, and tubes with low predicted values of reduced effective crossflow velocity did not undergo instability during the flow tests. The excellent agreement was true for both test configurations. In this subsection a quantitative evaluation of the results will be attempted. In particular, results from the subject prediction method will be compared with values of critical reduced flow velocity obtained from application of the most recent design guide and design data to the test heat exchanger.

Application of the stability diagram given in Fig. 1, or the stability criteria given in Table 1, to obtain the reduced critical flow velocity requires computation of the mass-damping parameter. For the subject test heat exchanger, with Admiralty brass tubes and water as the shellside fluid, the in-fluid mass per unit length (m) for the tubes is 0.0634 lb/in. The mass calculation is based on an added mass correction factor of 1.714 which takes into account the proximity to surrounding tubes in the tube bundle but does not account for coupling with adjacent tubes (adjacent tubes are assumed to be rigid). Attempts to measure equivalent viscous damping factors for the tubes were only partially successful [5,7]. However, based on the results obtained, it seems reasonable to assume a damping factor $\zeta = 0.035$. With these data as input, a mass-damping parameter for the tube bundle is computed as

$$\delta_m = \left(\frac{2\pi\zeta m}{\rho d^2}\right) = 0.69 \ . \tag{10}$$

Entering the stability diagram of Fig. 1 with a mass-damping parameter of 0.69, and using the lower bound curve, obtains $\bar{U}_r = 1.6$ as the lower bound value for the dimensionless critical velocity. With the use of Eq. (4) we obtain $\bar{U}_{CR} = 1.2$. A similar result is obtained by applying the lower bound stability equations given in Table 1. From Table 1, the lower bound stability criteria for a 30° triangular array and $(0.1 < \delta_m < 2)$ is

$$\bar{U}_{CR} = 3.58\ (P/d - 0.9)\delta_m^{0.1} \ . \tag{11}$$

For the subject test heat exchanger, with $P/d = 1.25$ and $\delta_m = 0.69$, we, again, obtain $\bar{U}_{CR} = 1.2$.

It is observed that there is considerable scatter in the data for low values of mass-damping parameter; Chen attributes this, in part, to the fact that the various experimenters were not consistent in their use of the pertinent parameters, mixing in-water and "in-vacuo" (in-air) values [27]. If the two lowest values (both attributed to Zukauskas and Katinas) were neglected, the lower bound curve established by Chen undoubtably would have been raised. In fact, a horizontal line intersecting the vertical axis at a value of approximately 2.2, giving $\bar{U}_{CR} = 1.6$, would not be unreasonable (see Fig. 1); such a result would imply that the dimensionless critical velocity is essentially independent of mass-damping parameter for triangular arrays in the low mass-damping parameter range. If the lower bound approach is not employed, and one simply uses the experimental data, accounting for the scatter, one might select a value of 2.8 for the dimensionless critical velocity. With Eq. (4), this yields $\bar{U}_{CR} = 2.1$.

In summary, the following values have been determined for the critical reduced flow velocity based on the stability diagram and lower bound stability criteria of Chen [22]:

$$\bar{U}_{CR} = \begin{cases} 1.2, \text{ based on lower bound stability curve (Fig. 1) and lower bound stability equation (Table 1)} \\ 1.6, \text{ based on revised lower bound stability curve (See Fig. 1)} \\ 2.1, \text{ based on experimental data (See Fig. 1) .} \end{cases} \quad (12)$$

There is obviously conservatism in the lower bound approach. While such conservatism is important from a designer's standpoint, for the purpose of evaluating a prediction method the most "realistic" value should be employed. With regard to neglecting the two low data points of Zukauskas and Katinas, it should be noted that, in general, the data of Zukauskas and Katinas may be considered suspect since they deviate significantly from expected trends; that is, they show a definite decreasing trend with increasing value of mass-damping parameter. In consideration of the above, the critical reduced crossflow velocity, for comparison with predicted values, will be taken as 2.1 based on the average of the experimental data, and assumed to be effectively independent of the mass-damping parameter.

The predicted values of reduced effective velocity as given in the tube mappings of Figs. 15 and 16 are for specified flow rates of 3,300 gpm (seven-baffle configuration) and 2,000 gpm (five-baffle configuration), respectively. These flow rates were selected as values close to the experimentally determined values for critical flow rate. The experimental results are summarized in Table 5, where ranges on measured critical flow rate are given along with average values. Since the critical flow rates are close to the

Table 5. Experimentally-determined values of critical flow rate and extrapolation factor K' based on the average critical flow rate

HX Configuration	Near Window		Far Window	
	Q_{CR} (gpm)	K'	Q_{CR} (gpm)	K'
7-Baffle	3,430-3,760		3,130-3,250	
	3,595	1.09	3,190	0.96
5-Baffle	2,790-3,000		1,970-2,140	
	2,895	1.45	2,055	1.03

flow rates specified in the two examples of application, it is reasonable to linearly extrapolate the computed results to estimate what the predicted reduced effective crossflow velocities are at the average values of the experimentally determined critical flow rates. This extrapolation can be accomplished as follows

$$\bar{U}_n\Big|_{Q=Q_{CR}} = K' \bar{U}_n\Big|_{Q=Q_{ref}} \tag{13}$$

where

$$K' = Q_{CR}/Q_{ref} ,$$

and

$$Q_{ref} = \begin{cases} 2{,}000 \text{ gpm, 5-baffle configuration} \\ 3{,}300 \text{ gpm, 7-baffle configuration} . \end{cases}$$

The appropriate values of the extrapolation factor K', based on the average value of critical flow rate, are given in Table 5.

In Figs. 20 and 21, the predicted values of reduced effective flow velocity, extrapolated to the averaged measured critical flow rates at which tubes in the near and far window regions are observed to first go unstable, are mapped. From the applicable stability diagram (Fig. 1) and experimental data from laboratory tests, contained in the stability diagram, it was determined that the tubes can be expected to go unstable when the reduced effective flow velocity exceeds the threshold value of approximately 2.1. We can see from Figs. 20 and 21, and a comparison between the reduced effective crossflow velocities (at the critical flow rate for a particular tube bundle configuration and particular window region) and the critical reduced effective crossflow velocity from the stability diagram, 2.1, that there is, in general, very good quantitative agreement. This is especially true for the far window regions of both tube bundle configurations and for the near window region of the five-baffle configuration; for the tubes in the row adjacent to the baffle cut, the predicted reduced effective flow velocities at the pertinent critical flow rate are in the range of 1.86 to 2.44. In the near window region of the seven-baffle configuration, four of the tubes adjacent to the baffle cut have predicted reduced effective flow velocities greater than or equal to 1.84.

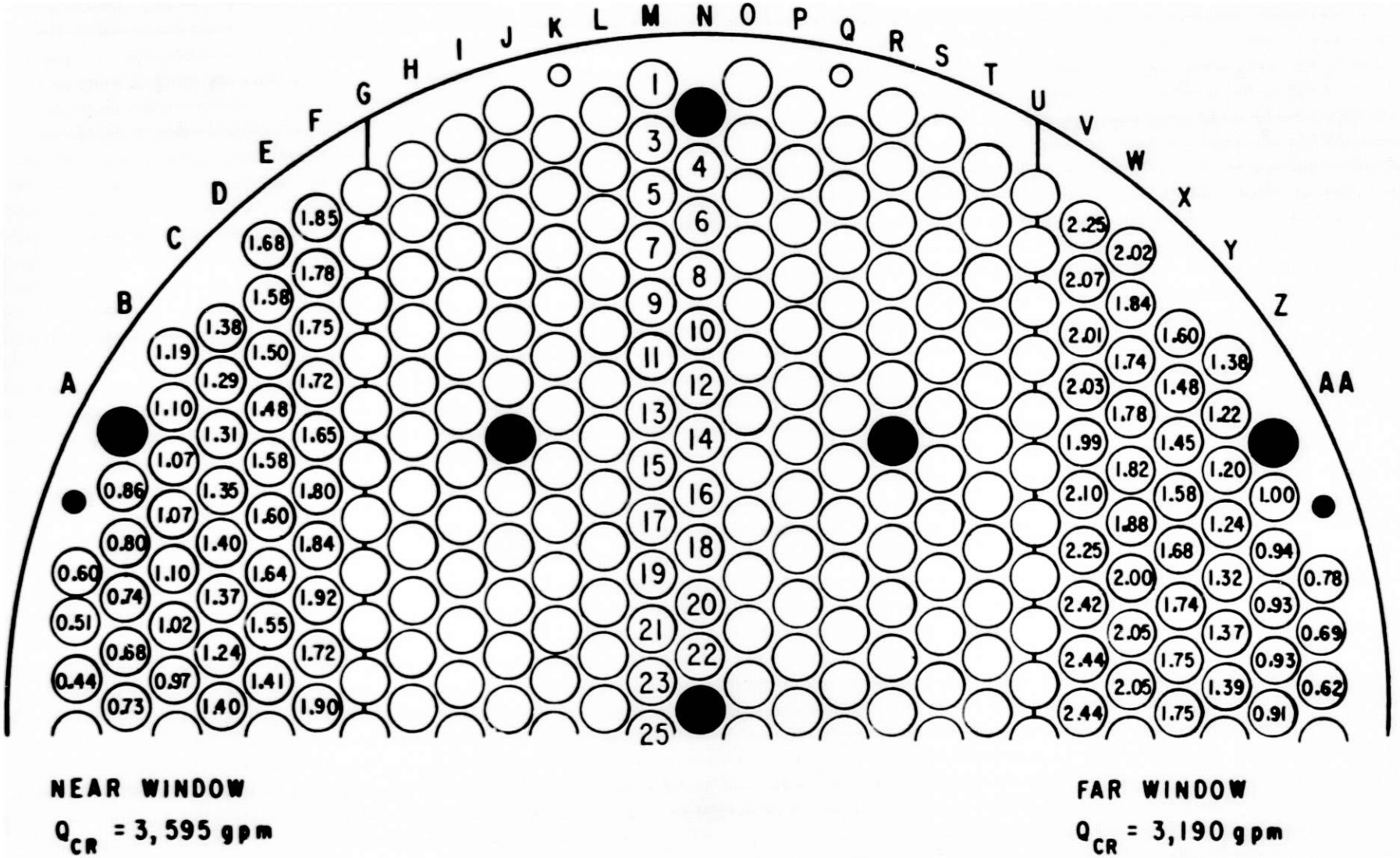

Fig. 20. Predicted values of reduced effective flow velocity extrapolated to average critical flow rate for the particular window region; 7-baffle configuration

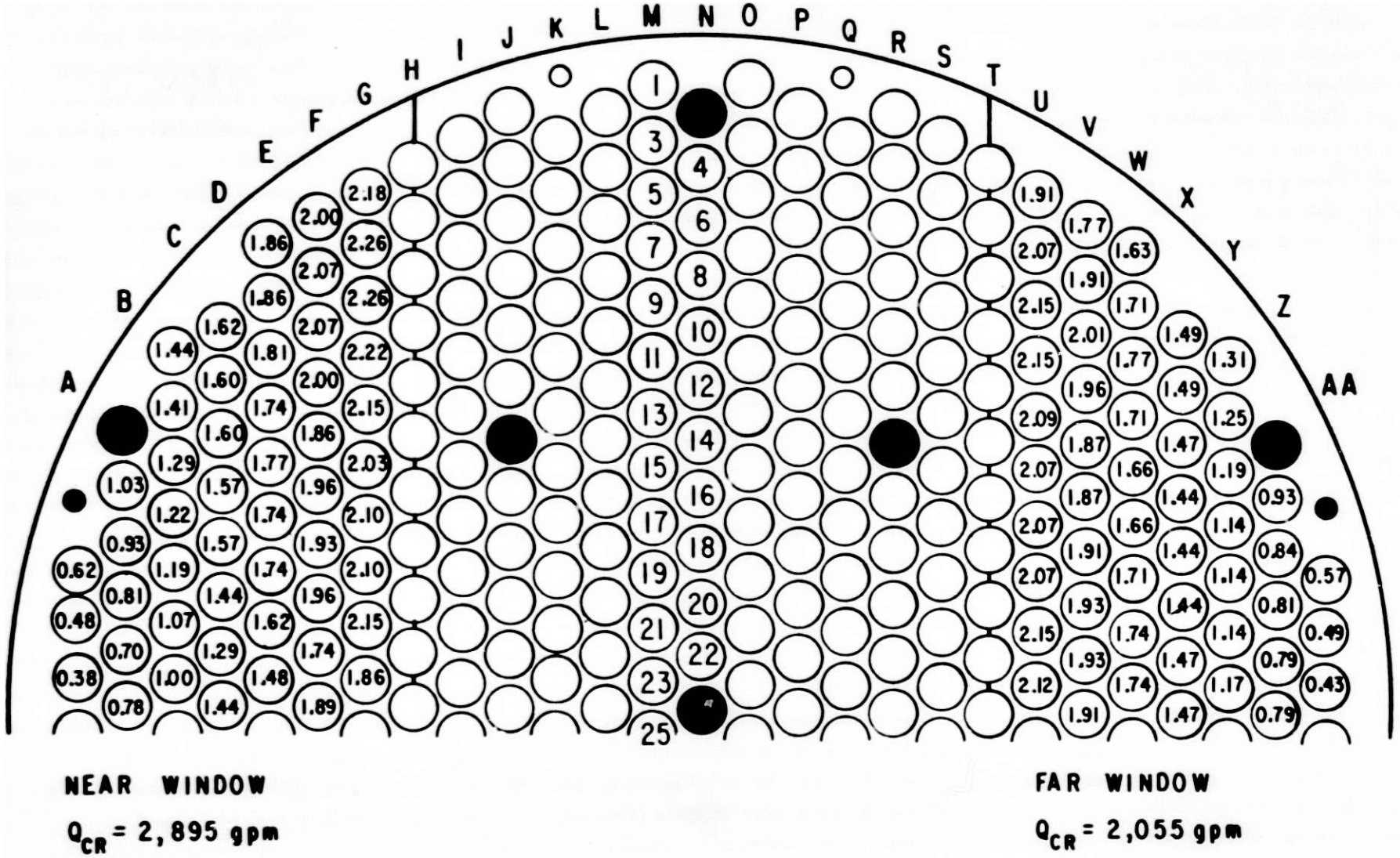

Fig. 21. Predicted values of reduced effective flow velocity extrapolated to average critical flow rate for the particular window region; 5-baffle configuration

VI. CONCLUDING REMARKS AND RECOMMENDATIONS

The framework for a computer-based method for predicting fluidelastic instability in heat exchanger tube bundles has been developed and presented. The method was applied to two different configurations of the Argonne test exchanger and evaluated qualitatively, by comparisons of predicted results with test observations, and quantitatively, by comparisons of results with critical values of reduced flow velocities as determined from a recent design guide. In both comparisons, excellent agreement was achieved, considering the overall complexities of the physical system and the fluidelastic instability mechanism itself. At this time, the method shows promise as a predictive tool for use in the evaluation and, ultimately, optimization of heat exchanger designs. However, additional development and evaluation is required.

Additional work is required in the following areas:

(1) First, and most importantly, there is the need to further evaluate the method by comparison with results from tests of different tube bundle configurations. Test data for this purpose are already available from the Argonne Heat Exchanger Tube Vibration Program [5,7,28]. The additional test data include full tube bundles on square and rotated square layouts [28], for both eight- and six-crosspasses, and several design fixes involving passlanes in the window region(s) [7]. In particular, the ability of the proposed method to predict the behavior of a tube bundle containing a passlane(s) would be very convincing evidence of its general validity and potential as a prediction tool.

(2) To make the method more readily usable by heat exchanger designers, there is the need to develop a "pre-processor" program that will generate the input (type and format) required by the COMMIX-IHX/SG code. This input data generator would have as its input basic heat exchanger dimensions such as tube diameter, tube bundle layout, pitch-to-diameter ratio, baffle spacing, baffle cut, shell inside diameter, nozzle diameters, and the like. (It should be noted that the first version of such a program has been written.)

(3) The "post-processor" program, which is in effect the vibration analysis, should be extended to have the computer calculate the reduced effective flow velocities and plot the various maps of reduced velocities as given, for example, in Figs. 15 and 16. (Here, also, a first version of such an expanded post-processor program has been written.)

(4) The COMMIX-IHX/SG code includes a transient sweep capability. In application, transient inlet conditions are specified for the length of the run, varying continuously throughout. To take advantage of this feature, a new heat exchanger might be subjected to increasing flow, from low flow rates

to well over the projected flow at which high tube vibration and impacting would occur. At intervals along the transient, restart tapes or plot tapes might be written. These tapes could then be analyzed by the present method to give a series of "snapshots" of tube vibration along the flow sweep.

(5) The COMMIX-IHX/SG code includes heat transfer, as well as tubeside two-phase flow, capabilities. Assuming one is interested in flow distribution only, the code could be simplified to run more economically. However, arguments can be made (see Item 6, below) for retaining the thermal capabilities of the code.

(6) The thermal analysis capabilities of the code could also be utilized. Among other things this would permit evaluation of differential thermal expansion as it effects tube vibrational characteristics and response. Techniques for optimizing tube bundle configurations, baffle placement, and inlet velocities might then be developed. In short, an accurate tube vibration optimization tool might be developed.

ACKNOWLEDGMENTS

The authors gratefully acknowledge D. E. Foulser who, working as a student research associate for the summers of 1980 and 1981, applied the COMMIX-IHX/SG code to the test exchanger, wrote required pre- and post-processor programs, and performed the computer computations; S. S. Chen for numerous discussions on fluidelastic instability in tube bundles and for review and comments on the subject report; H. H. Chung for his help in implementing the BEAMINT code; and R. C. Schmitt for general consultation on the use of the COMMIX-IHX/SG code and for the computer graphics depicting flow patterns.

REFERENCES

1. Wambsganss, M. W., Halle, H., and Chenoweth, J. M., "A DOE-Sponsored Program on Heat Exchanger Tube Vibration," Proc. 16th Intersociety Energy Conversion Engineering Conference, Vol. 1, pp. 595-599, ASME (1981).

2. Pettigrew, M. J., and Ko, P. L., "A Comprehensive Approach to Avoid Vibration and Fretting in Shell-and-Tube Heat Exchangers," ASME Pressure Vessel and Piping Conference, San Francisco, August 13-15, 1980.

3. Connors, H. J., "Flow Induced Vibration and Wear of Steam Generator Tubes," Nucl. Tech. 55, 311-331 (1981).

4. Collinson, A. E., and Taylor, A. F., "A Development Programme for the Minimisation of Vibration in a U-Tube Steam Generator Bundle for an LMFBR," Paper No. 2.1 in Proc. UKAEA/BNES Third Keswick Int'l Conf. on Vibration in Nuclear Plant, Keswick, U.K., May 1982.

5. Halle, H., and Wambsganss, M. W., "Tube Vibration in Industrial Size Test Heat Exchanger," ANL-CT-80-18, March 1980.

6. Halle, H., Chenoweth, J. M., and Wambsganss, M. W., "Flow-Induced Tube Vibration Tests of Typical Industrial Heat Exchanger Configurations," ASME Paper No. 81-DET-37, 1981.

7. Wambsganss, M. W., Halle, H., and Lawrence, W. P., "Tube Vibration in Industrial Size Test Heat Exchanger (30° Triangular Layout - Six Crosspass Configuration)," ANL-CT-81-42, October 1981.

8. Chen, Y. N., "The Sensitive Tube Spacing Region of Tube Bank Heat Exchangers for Fluidelastic Coupling in Cross Flow," ASME Paper No. PVP-PB-026, 1977.

9. Connors, H. J., Jr., "Fluidelastic Vibration of Tube Arrays Excited by Cross Flow," in Flow-Induced Vibration in Heat Exchangers, (ed. D. D. Reiff), pp. 47-56, ASME, New York, 1970.

10. Weaver, D. S., and Grover, L. K., "Cross-Flow Induced Vibrations in a Tube Bank - Turbulent Buffeting and Fluid Elastic Instability," J. Sound Vib. 59, 277-294 (1978).

11. Zukauskas, A., and Katinas, V., "Flow-Induced Vibration in Heat-Exchanger Tube Banks," in Practical Experiences with Flow Induced Vibrations, (eds. E. Naudascher and D. Rockwell), pp. 188-196, Springer-Verlag, Berlin, 1980.

12. Soper, B. M., "The effect of Tube Layout on the Fluidelastic Instability of Tube Budnles in Cross Flow," in Flow-Induced Heat Exchanger Tube Vibration - 1980, HTD-Vol. 9, pp. 1-9, ASME, New York, 1980.

13. Blevins, R. D., Gibert, R. J., and Villard, B., "Experiments on Vibration of Heat Exchanger Tube Arrays in Cross Flow," Paper B6/9, in Trans. 6th International Conference on Structural Mechanics in Reactor Technology, Paris, 1981.

14. Chen, S. S., and Jendrzejczyk, J. A., "Experiments on Fluid Elastic Instability in Tube Banks Subjected to Liquid Cross Flow," J. Sound Vib. 78, 355-381 (1981).

15. Heilker, W. J., and Vincent, R. Q., "Vibration in Nuclear Heat Exchangers due to Liquid and Two-Phase Flow," ASME J. Eng. for Power 103, 358-366 (1981).

16. Yeung, H. C., and Weaver, D. S., "The Effect of Approach Velocity Direction on the Flow-Induced Vibrations of a Triangular Tube Array," ASME J. Mech. Design 104 (1982).

17. Tanaka, H., and Takahara, S., "Unsteady Fluid Dynamic Force on Tube Bundle and Its Dynamic Effect on Vibration," in Flow Induced Vibration in Power Plant Components (ed. M. K. Au-Yang), PVP-Vol. 41, pp. 77-92, ASME, New York, 1980.

18. Chen, S. S., "Instability Mechanisms and Stability Criteria of a Group of Circular Cylinders Subjected to Cross Flow. Part I: Theory," ASME Paper 81-DET-21; To appear in J. Vibration, Acoustics, Stress and Reliability in Design, Trans. ASME.

19. Chen, S. S., "Instability Mechanisms and Stability Criteria of a Group of Circular Cylinders Subjected to Cross Flow. Part II: Numerical Results and Discussions," ASME Paper 81-DET-22; To appear in J. Vibration, Acoustics, Stress and Reliability in Design, Trans. ASME.

20. Price, S. J., and Paidoussis, M. P., "Fluidelastic Instability of an Infinite Double Row of Circular Cylinders Subject to a Uniform Crossflow," ASME Paper 81-DET-24; To appear in J. Vibration, Acoustics, Stress and Reliability in Design, Trans. ASME.

21. Lever, J. H., and Weaver, D. S., "A Theoretical Model for the Fluidelastic Instability in Heat Exchanger Tube Bundles," in Flow Induced Vibration of Circular Cylindrical Structures - 1982 (eds. S. S. Chen, M. P. Paidoussis, and M. K. Au-Yang), PVP-Vol. 63, pp. 87-108, ASME, New York, 1982.

22. Chen, S. S., "Design Guide for Calculating the Instability Flow Velocity of Tube Arrays in Crossflow," ANL-CT-81-40, December 1981.

23. Sha, W. T., Yang, C. I., Kao, T. T., and Cho, S. M., "Multidimensional Numerical Modeling of Heat Exchangers," ASME J. Heat Transfer 104, 417-425 (August 1982).

24. Shin, Y. S., Jendrzejczyk, J. A., and Wambsganss, M. W., "Effect of Tube-Support Interaction on the Vibration of a Tube on Multiple Supports," ANL-CT-77-8, January 1977.

25. Collinson, A. E., and Warneford, J. P., "Vibration Tests on Single Heat Exchanger Tubes in Air and Static Water," UKAEA/BNES Conference on Vibration in Nuclear Plant, Keswick, May 1978.

26. Chung, H. H., "Analysis Method for Calculating Vibration Characteristics of Beams with Intermediate Supports," ANL-CT-79-41, July 1979.

27. Chen, S. S., Personal communication, November 1982.

28. Halle, H., and Wambsganss, M. W., "Tube Vibration in Industrial Size Test Heat Exchanger (90° Square Layout)," ANL-83-10, February 1983.

Distribution for ANL-83-8

Internal:

J. J. Roberts
R. S. Zeno
G. S. Rosenberg
A. R. Evans
R. E. Holtz
W. T. Sha
M. W. Wambsganss (60)
B. L. Boers
A. R. Brunsvold
S. S. Chen
H. H. Chung
H. Halle (90)
J. A. Jendrzejczyk
W. P. Lawrence
T. M. Mulcahy
R. C. Schmitt
P. Turula
C. I. Yang (3)
M. Weber
ANL Patent Dept.
ANL Contract File
ANL Libraries (3)
TIS Files (6)

External:

DOE-TIC, for distribution per UC-95f (249)
Manager, Chicago Operations Office, DOE
Director, Technology Management Div., DOE-CH
D. L. Bray, DOE-CH
Components Technology Division Review Committee:
A. A. Bishop, U. Pittsburgh
F. W. Buckman, Consumers Power Co.
R. Cohen, Purdue U.
R. A. Greenkorn, Purdue U.
W. J. Jacobi, Westinghouse Electric Corp., Pittsburgh
E. E. Ungar, Bolt Beranek and Newman, Inc., Cambridge, Mass.
J. Weisman, U. Cincinnati